Journal of Non-Crystalline Solids 43 (1981) 37–77

TOPOLOGY OF COVALENT NON-CRYSTALLINE SOLIDS II: MEDIUM-RANGE ORDER IN CHALCOGENIDE ALLOYS AND A-Si(Ge)

J.C. PHILLIPS
Bell Laboratories, Murray Hill, New Jersey 07974, USA

Received 23 October 1979
Revised manuscript received 9 October 1980

Characteristic order over distances of 15–30 Å is indicated by various experiments on covalent non-crystalline solids. The data are reviewed and detailed structural models are developed containing 30–1000 atoms.

1. Introduction

Historically the metastability of glasses has been discussed from many different viewpoints (the early history is reviewed in ref. [1]). In the early 1930s Simons introduced a kinetic approach. He distinguished between the measured glass transition temperature $T = T_g$, at which the supercooled liquid freezes with rapid drops in specific heat, thermal expansion, compressibility, etc., and the ideal glass transition temperature T_0 obtained from the viscosity η which is fitted very well by $\ln \eta = A/(T - T_0)$. In 1948 Kauzmann pointed out [2] * that thermodynamically certain glass transition temperatures T_x could be defined by linear extrapolation of the "configurational" quantities $\Delta X = X$ (liquid) $- X$ (crystal) to zero. For X we can choose entropy S, enthalpy or internal energy H, or volume V. On the basis of the fragmentary (and in reality inconclusive) data available at that time Kauzmann guessed that $T_0 = T_s$. The conjecture was based on a hypothetical configurational third law of thermodynamically metastable systems; in effect, Kauzmann observed that it would be absurd to have $\Delta S < 0$, thus as $\Delta S \to 0+$ we approach an "entropy crisis" which is resolved by the glass transition.

* The formal discussion of constraints in statistical mechanics is at present in an elementary state. However, it has been recognized that the use of rigid mechanical constraints can lead to paradoxical results, and that satisfactory results are obtained when the flexibility of the constraints is included, i.e., when allowance is made for vibrational entropy. (Our discussion frequently emphasizes the vibrational entropy associated with internal surfaces.) For a recent formal discussion see Fixman [2].

The chemical systematics of glass formation also suggest that $T_0 = T_s$. If we define the quality of a glass in terms of the inverse of its minimal quenching rate, i.e., the slowest cooling rate which can be employed without crystallization of the supercooled liquid, then the best (smallest minimal quenching rate) inorganic glasses are formed from materials with network (covalently bonded) structures. Such structures have low coordination numbers and lower densities than non-covalently bonded systems. (At the opposite extreme we have close packed systems such as the rare gases or some metals, many of which have never been quenched rapidly and homogeneously enough to form glasses. The materials may have been, e.g. evaporated or splat-quenched to form disordered solids, but upon heating the samples nearly always recrystallize before passing through a glass transition. The term amorphous is reserved explicitly for materials which in bulk recrystallize before undergoing a glass transition.)

Intuitively it may be felt that the essential features of network structures are combinatorial in nature and are contained, e.g., in ring statistics describing ring size, number of interlocking rings, etc. If this were so then the relevant configurational variable determining the glass transition would be $X = S$, and thus chemical justification for assuming that $T_0 = T_s$ would be obtained. By now there is abundant experimental evidence [3] from polymer glasses that $T_0 = T_s$ and that T_H, $T_V \lesssim 3T_0/4$, and (though with less confidence, because a greater extrapolation is involved) $T_H \simeq T_V$. This suggests that elaboration and refinement of our intuition concerning the network basis of glass formation is appropriate.

In an earlier paper [4] (hereafter referred to as I) some reasons were given for studying theoretically alloys of Ge–As–(S, Se), which formed chalcogenide glasses. Experimentalists have noted that these alloys form solid solutions over a wide range of composition, and that the properties important for glass formation (such as viscosity) appear to depend primarily [4] on the average coordination number m, especially when $0 \lesssim m - 2 \lesssim \frac{1}{2}$. In I the role played by short-range order, and specifically by m, was examined in some detail.

The central idea in I was that Kauzmann's macroscopic and thermodynamical identification of T_0 with T_s could be justified microscopically and statistically in chalcogenide glasses. In these materials the interatomic forces are predominantly covalent (in contrast to the oxide glasses, where ionic forces are also significant) and of short range. It then became possible to classify the interatomic forces into strong and weak forces, and to show (e.g., from radial distribution functions as measured in diffraction experiments) that the strong forces act as mechanical constraints (see Kauzmann [2] and previous footnote) in network formation; the weak forces (such as van der Waals polarization interactions) played little role in I, but their role here, in our discussion of medium-range order, is more substantial. The discussion given in I of the optimal glass-forming composition in chalcogenide alloys constitutes the first quantitative microscopic realization of Kauzmann's macroscopic conjecture. It was also shown that when the number of constraints per atom exceeded the number of degrees of freedom, that the constraints were separa-

ble into two groups, *intact* and *excess*. Moreover the excess constraints were broken, with an attendant increase in strain energy. The latter can be described as anharmonic or configurational strain energy [4], and it manifests itself, e.g., by a broadening of the more distant (A–A or B–B, as the case may be) component of the split second-neighbor peak in AB_2 glasses such as SiO_2, or more particularly, $Ge(S, Se)_2$. Our central result was that the best glasses were to be found at the "perfect glass" composition $x = x_c$ where the number of constraints exactly equalled the number of degrees of freedom, so that only residual van der Waals interactions were contributing to the configurational strain energy.

It is obvious that near $x = x_c$ unusual behavior may be expected in the glass, i.e., the perfectly matched short-range forces may generate anomalously extensive medium-range order. In this paper we discuss the nature of medium-range order in perfect (or near-perfect) glasses. Some extensions of these ideas are made to amorphous materials, and a structural model is proposed which differentiates between network substances according to whether they are amorphous or glassy in bulk.

2. Topological definitions

Many experiments have suggested that the range R of atomic order in glasses and glass-forming supercooled liquids is much longer than in normal liquids near and above $T = T_m$. To describe this order earlier authors often used geometrical models. (For example, to explain the relative slowness of crystallization of glass-forming supercooled liquids it has often been proposed that monomeric clusters are present. These clusters may be special polyhedra with point symmetry elements, such as five-fold rotation axes, which are not easily assimilated into space groups [5].) Recently, however, geometrical descriptions of chalcogenide glass structures have fallen out of favor. In binary alloys Lucovsky and co-workers, for example, have stressed the importance of chemical ordering (alternation of cations and anions wherever possible) but have otherwise used combinatorial arguments to estimate cluster concentrations [6]. This is a useful refinement of the "random network" concept, but it leaves open the fundamental questions involving embedding the clusters in a continuous network, i.e., it does not address the problem of reconciling clusters with connectivity.

In I of this series we saw, in discussing the glass-forming tendencies of Ge_ySe_{1-y} alloys (see fig. 1 of I), that connectivity was probably of more significance kinetically than the local structure of clusters, except in the immediate vicinity of crystalline compositions, $y = 0$ and $y = \frac{1}{3}$. The question then arises, is more than one kind of connectivity possible? Which kinds actually occur in chalcogenide glasses? The following topological definitions will be useful in discussing alternative forms of medium-range order in chalcogenide classes.

Consider any chain of four covalently bonded atoms (4-chain). Construct the plane which most nearly contains these atoms (i.e., minimize the distance of the

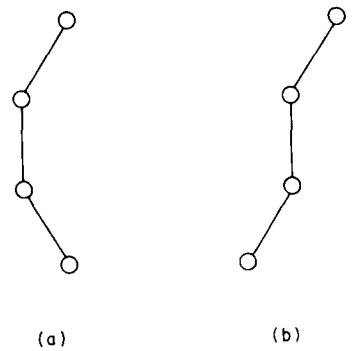

Fig. 1. Possible conformations of 4-atom chains: (a) eclipsed (c); (b) staggered (o).

atoms to the plane). Denote the unit normal to this plane by $\boldsymbol{n}$. In the plane construct the vector $\boldsymbol{d}$ which most nearly contains the projected coordinates. If we examine the projected coordinates in the plane of the 4-chain, we see that there are two possible conformations of atoms 1 and 4 relative to 2 and 3; 1 and 4 both lie on the same side of 2 and 3, fig. 1(a) or on opposite sides, fig. 1(b); the two possibilities correspond to more nearly eclipsed and more nearly staggered conformations of the dihedral angle in conventional molecular terminology. The first conformation indicates the beginning of a chain that may close on itself (c) to form a ring, the second conformation indicates an open chain (o). Because in glass-forming materials the bond-bending constraints match in number the available degrees of freedom, these tendencies may persist over several adjacent chain segments, so that $\boldsymbol{n} \cdot \boldsymbol{n}' \simeq 1$, where $\boldsymbol{n}$ and $\boldsymbol{n}'$ are the unit normals associated with adjacent chain segments, and similarly the segements are paired preferentially, i.e., open/open (o, o) or closed/closed (c, c) pairs are more probable than open/closed (o, c) pairs. The reason for this, of course, is that (o, o) and (c, c) pairs can be packed more densely than (o. c) pairs [figs. 2(a), (b) and (c)] and therefore can take better advantage of

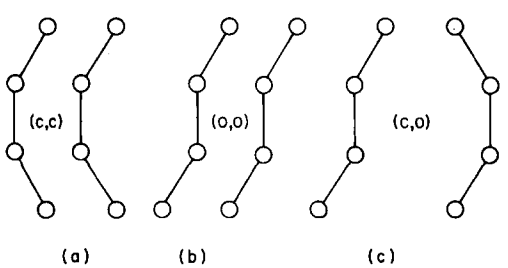

Fig. 2. Possible packings of pairs of conformations of 4-atom chains: (a) eclipsed–eclipsed (b) staggered–staggered; and (c) eclipsed–staggered. Note that (a) and (b) are more compact than (c), and hence have lower van der Waals energies.

the lone pair van der Waals energies. The vectors $\boldsymbol{n}$ and $\boldsymbol{d}$ are the local directrices of the local polymeric texture.

Next we must examine the 4-chains in the plane with normal $\boldsymbol{u} = \boldsymbol{n} \times \boldsymbol{d}$. Again we have two possibilities for atoms 1 and 4 compared with 2 and 3, namely open ($\overline{\text{o}}$) and closed ($\overline{\text{c}}$). In three dimensions helical chains contain only [o, $\overline{\text{o}}$] segments; one form of crystalline Se contains arrays of helical chains. Puckered rings with atoms alternately in two closely spaced planes are of the type [c, $\overline{\text{o}}$]; other crystalline forms of Se contain segments of only this type. Thus characterizing the 4-chains in two perpendicular planes ($\boldsymbol{n}$ and $\boldsymbol{u}$) exhausts all possibilities and determines the medium-range order (which may also be described as the local polymeric texture) of the network. At present it is believed [7] that glassy S and Se contain both kinds of 4-chains.

What kind of medium-range order do we expect to find in compounds such as $GeSe_2$ and As_2Se_3? At low concentrations $0 \lesssim x, y \lesssim 1$ in As_xSe_{1-x} and Ge_ySe_{1-y} alloys the addition of As($N_{cn} = 3$) and Ge($N_{cn} = 4$) is commonly described by terms such as "branched chains." However, we have already seen in I, fig. 7, that this nomenclature is inadequate, because $As_{2y}Se_{1-2y}$ is topologically homologous to Ge_ySe_{1-y}. At a minimum this means that As atoms occur predominantly in enantiamorphic pairs of some Kind, =As––?––As= which are topologically equivalent to =Ge= atoms What is the topological origin for this behavior?

In I we suggested that As atoms could be paired through an intermediate Se atom, i.e., the pairs form =As–Se–As= units (I, fig. 8). In terms of the enthalpy of a network of atoms bonded by covalent (short-range) forces only, this explanation is not implausible. However, the configurational entropy of such a specific structure seems too small for the liquid state or a glass. The configurational entropy is much greater in bundles of parallel chains. If we taken into account the van der Waals attraction between bundled branched chains, the structure shown in fig. 3 appears

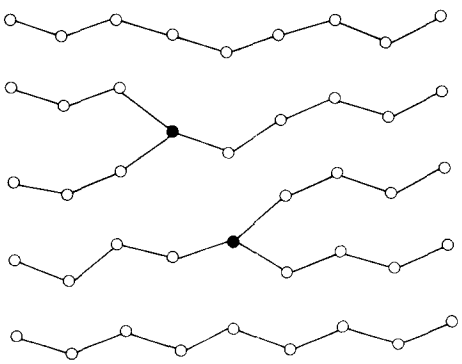

Fig. 3. Probable nature of medium-range order in As_xSe_{1-x} glasses with $x \lesssim 0.1$. The As atoms act as branching points of Se chains; by pairing these branching points the van der Waals energy is lowered; cf. fig. 2.

to be a great improvement over I, fig. 8. The polymerized quasi-linear texture of parallel chain bundles is retained in spite of the branching at the As atoms because of the indicated pairing, ensuring a large van der Waals attractive interaction. Thus the *medium-range order* between disconnected parts of the network *is mediated by non-bonding interactions.*

The reader who is familiar with dislocation interactions in ferroelectrics will recognize in fig. 3 a structure which is very similar to the alignment of domain wall tips ("domain wall freezing", a phenomenon in some respect quite similar to the glass transition) which has been observed directly by Bornarel [8]. This typically occurs at a temperature T_p^* which is of order (0.5–0.7) T_c, compared with T_g, which is of the order of (0.6–0.8) T_m Thus the Curie temperature T_c plays the role of the melting point of the crystal T_m while the "freezing" of the supercooled liquid into a structure with medium-range order (paired brnaching centers) occurs at T_p^* or T_g.

In this example we already recognize certain factors which will play important roles in the structures discussed below. The network structure of the glassy alloy reflects, in general, the texture and dimensional character of the crystalline structures which lie nearest in composition. This tule may be ambiguous (are As_xSe_{1-x} and Ge_ySe_{1-y} alloys for $0 \lesssim x, y \lesssim 0.4$ predominantly linear, like bundles of Se chains, or predominantly planar, like stacked units of Se_8 rings?) but it is always a useful improvement over superficial analogies, e.g. with SiO_2, which have generated phrases such as "random covalent network," which imply an isotropic, homogeneous, fully three-dimension character for network chalcogenide glasses. In fig. 3 because of medium-range order the As atoms are paired, i.e., it is necessary but not sufficient to assume merely that short-range chemical ordering has taken place and that cation/anion bonds are preferred whenever consistent with compositional limitations. Once the composition falls in a glass-forming region, if we perform any kind of experiment which yields qualitatively different results than we would have obtained for amorphous materials containing only short-range order, it is incumbent on us to seek topological origins for those results based on medium-range order.

We now examine evidence for medium-range order in $GeSe_2$ and As_2Se_3. This evidence demonstrates clearly that the range R of medium-range order in glasses at or near these compositions is far greater than would be expected from "random network" models, and that the local polymeric textures are anisotropic.

3. Anomalous first sharp diffraction peaks

The existence of a first sharp diffraction peak (FSDP) corresponding to molecular clusters with a center-to-center spacing S_c of 5 Å was first reported in the chalcogenide glass As_2Se_3 by Russian workers [9]. The peak is sufficiently narrow that it must be associated with a correlation length $R \sim 15$–20 Å. The anomaly has since

been widely studied by workers in many countries. It has been observed in $As_2S_3(Se_3)$ [10,11], $GeS_2(Se_2)$ [12,13] as well as elemental B, P, As and Sb [14]. It is not surprising that this peak has received so much attention because it is clearly the strongest and most universal signature of medium-range order and hence it may contain the secret of the pronounced glass-forming tendencies of covalent materials with average coordination number N_{cn} close to 2.5.

Is there a single simple explanation for the origin of this peak? In the early Russian work [9] it was supposed that evaporated films of As_2Se_3 contained deformed microcrystallites with a layer-like structure; the spacing between layers in the crystal is 5 Å, in good agreement with the measured values of S_c. However, subsequent studies of As_xSe_{1-x} alloys [10] showed that while S_c was independent of x, the intensity $I_c(x)$ of the peak reached its maximum value at $x = 0.5$, *not* $x = 0.4$, but that no correspondence could be established with microcrystallites of As_4Se_4. The layer model for the evaporated films has now been questioned both because of detailed diffraction analysis [10] and the correlation of the degrading effect of annealing on the diffraction peak and certain As–As vibration lines in the Raman spectrum [15].

A second model for the $As_2S_3(Se_3)$ peak involves polyhedral network fragments which are spheroidal in shape. The most symmetric of these is an $As_4S_5(Se)_6$ molecule with As atoms at the corners of a tetrahedron and S(Se) atoms situated above the six edges with a bond angle close to 100°. This model, however, also fails to explain the diffraction and Raman data [10,11,15]. The generally accepted model now is an As_4S_4 cluster, which can be regarded as a fragment of As_4S_6. with two S

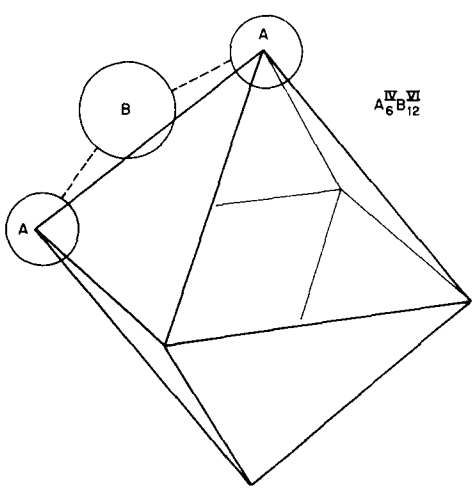

Fig. 4. A fully monomerized Ge_pSe_{2p} spheroidal hollow cluster with $p = 6$. This is a possible cluster in g-$GeSe_2$ from a topological point of view, but the strain energy at the Ge atoms is much too great. This structure must therefore be rejected.

atoms removed and two "long" As–As bonds [11]. These clusters may be partially polymerized with S chain fragments, but at the same time there may be cluster–cluster ordering on a scale of $R \sim 15$ Å.

The foregoing brief account of the emergence of a generally accepted explanation of the origin of medium-range order in evaporated $As_xS_x(Se_{1-x})$ alloys has summarized only a small amount of the effort which has been expended on this system. Granted, however, that As_4S_4 molecular units are stable in the vapor (and to a lesser extent in the supercooled liquid), how does this help us to understand the occurrence of a sharp first diffraction peak in Ge_ySe_{1-y} alloys, not to speak of a-B, P, As and Sb? It is true that [unlike $As_xS_{1-x}(Se_{1-x})$] $I_c(y)$ peaks at the $y = \frac{1}{3}$ in Ge_ySe_{1-y} alloys [12,16] but the smallest molecular cluster consistent with $N_{cn}(Ge) = 4$ and $N_{cn}(Se) = 2$ is a Ge_6Se_{12} unit of the kind shown in fig. 4. However, it has been shown [17] that the radial distribution function of such a cluster is not in good agreement with experiment for g-$GeSe_2$.

The viewpoint advanced in this paper is that the layer-like model is correct for g-$GeSe_2$, a B, P, As and Sb, and *liquid* As_2Se_3 (above $T = T_g$). Because so much effort has been expended to identify As_4S_4 molecular clusters in evaporated As_xS_{1-x} glasses our return to the original layer model in other materials may seem anticlimatic. However, there is good evidence for the layer model both from diffraction and Raman data.

Let us consider the diffraction data first. Because the molecular clusters are so large there is not enough information in the diffraction spectrum alone to enable us

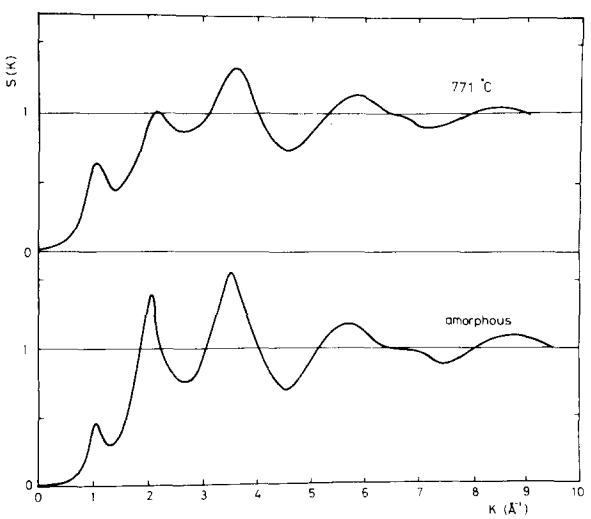

Fig. 5. The radial diffraction pattern for g-$GeSe_2$ from room temperature to above the melting point of the crystal (= 740°C), taken from ref. [13] and reproduced here for the reader's convenience.

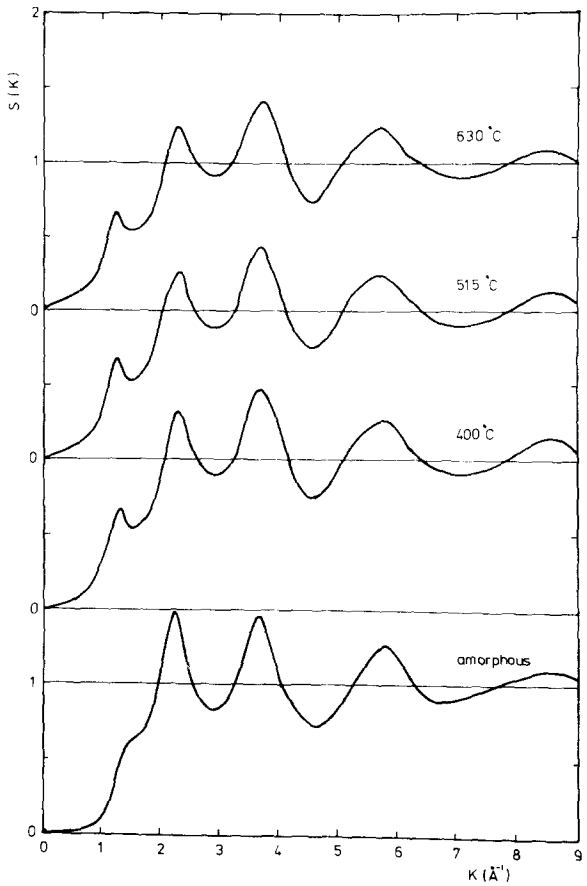

Fig. 6. The radial diffraction pattern for g-As_2Se_3 from room temperature to above the melting point of the crystal (= 380°C), data again taken from ref. [13].

to invert the data and to determine the structure. What are needed are qualitative features that can be used to differntiate $GeSe_2$ from As_2Se_3 and to supplement the quantitative diffraction analysis of first and second neigbor positions. Recently dramatic data have appeared [13] showing the diffraction patterns of As_2Se_3 and $GeSe_2$ at temperatures up to $T = 1.5T_m \simeq 2T_g$. These data are reproduced, for the reader's convenience, in figs. 5 and 6.

The relative transition temperatures for melting of the glass and crystal (T_g, T_m) are (422, 740) for $GeSe_2$ [18] and (170, 380) for As_2Se_3 [19] in °C. In fig. 5 the data for $GeSe_2$, taken at $T = 771°C > T_m$, show that apart from a small amount of broadening the anomalous FSDP near $K = 1.0$ (Å^{-1}) is unchanged on going from the glass to the normal liquid. *This is conclusive evidence that the FSDP is not associated with microcrystallites.*

The origin of the peak must be based on the presence of large molecular clus-

ters with a center-to-center spacing $S_c \sim 6$ Å. If these clusters are quasi-planar a correlation length R normal to planes can be estimated from the peak width [20]

$$R/r_0 = q_1/\Delta q_1,$$

where r_0 is the interlayer spacing and Δq_1 is the half-width of the FSDP at $q = q_1$. If the clusters are spheroidal a random-acking model can be used, although the inferred packing densities [11] of order 0.5–0.6 seem too low, i.e., the packing is probably not random. In the layer model it appears that R/r_0 decreases from 10 in the glass to 5 at $T = T_m+$ in $GeSe_2$.

The results for As_2Se_3, which are shown in fig. 6, are much more interesting and appear to give evidence for a *structural transition*. At $T = 630°C = 900$ K $= 2.2T_g = 1.4T_m$ an FSDP is present near $K = 1.0$ Å^{-1}. At $400°C = 1.03T_m$ the peak has shifted to 1.2 Å^{-1} and for $T < T_g$ it has shifted even further to 1.4 Å^{-1}. Ordinarily we do not expect to observe the formation of molecular structures as precursors [21] to *first order* phase transitions, i.e. the crystallization at $T = T_m$. However, an exception to this thermodynamic principle might be found in a glass-forming material where the molecular structure of the glass resembled that of the crystal. It is not unreasonable to suppose that quasi-planar As_6Se_6 rings exist at high T in the liquid and are spaced about 7 Å apart. As T is lowered, the rings (and their peripheral Se outriggings) become more symmetric, with a reduced spacing of 5 Å between adjacent layers. Thus, the change in the intercluster spacing reflects a change in intra-ring structure. At high T the rings may be stacked but partially rotated relative to one another about the common normal. As T is reduced the rotational disorder decreases which would help to explain the remarkable data shown in fig. 6. The reader should note that Nemanich et al. found positive evidence for As_4S_4 clusters in thin films but were able to conclude only that some kinds of clusters (unspecified) were present in As_xSe_{1-x} alloys [15].

One of the greatest obstacles to the analysis of medium-range order in non-crystalline solids has been the assumption on the part of many workers that because so many atoms (~30–1000!) are involved there cannot be enough information in the data to determine the structure. In general this view is valid. However, to the extent that the data contain certain anomalous features, we may hope to establish corresponding structural properties by dint of combining all the data available on structurally related material. (Before Bragg this procedure was used to guess the structures of many crystals and molecules, and it was quite successful in the hands of a few skilled individuals, although of course this approach cannot be automated.) We now utilize this approach to develop detailed molecular models for g-$GeSe_2$ and g-As_2Se_3.

4. The Companion A_1 Raman peak in g-$GeSe_2$

Infrared and Raman spectra provide additional information on the structure of molecular clusters found in glasses. By comparing the glassy spectra with crystalline

Table 1
Raman frequencies in GeX_2 glasses (X = S, Se, Te) in cm^{-1}. Data from Kumagi et al. [23] and ref. [34]. The value of ν_4 is taken from infrared measurements, but in $GeTe_2$ only it is also observed in the Raman spectrum

Material	$\nu_1(A_1)$	ν_c	$\nu_2(E)$	$\nu_3(F_2)$	$\nu_4(F_2)$
GeS_2	342	385	105	375	149
$GeSe_2$	198	212	82	(257, 304)	100
$GeTe_2$	167	absent	80	230	131

spectra and by utilizing quasi-selection rules regarding infrared versus Raman activity we may be able to identify local vibrational modes in the glass which are also present in the crystal. In general, of course, these local modes contain information about short-range order only. However, in a few exceptional cases anomalous dependences on composition are found which are indicative of the presence of substantial medium-range order.

The most spectacular example of a Raman line which is the signature of medium-range order was discovered by French workers [22] in g-$Ge_y(Se_{1-y})$ alloys. For $0 < y \leqslant \frac{1}{3}$ the dominant structural units in these glasses are probably $Ge[S_{1/2}(Se_{1/2})]_4$ tetrahedra which are polymerized with S(Se) chain fragments. Both the chains and the tetrahedra produce local phonon modes which are easily identified in the spectra through their dependence on composition, anion mass, relative infrared- and Raman-activity, and finally (in the case of the tetrahedra) by comparison with the

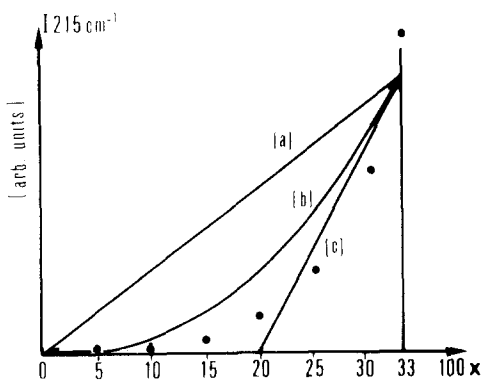

Fig. 7. The intensity $I(A)$ of the Raman scattering from the A_1 (215 cm^{-1}) mode of $Ge(Se_{1/2})_4$ tetrahedral cluster follows the linear relation (a). Curves (b) and (c) represent unsatisfactory fits to $I_c(x)$, the composition dependence of the strength of the Raman scattering from the companian mode (represented by the experimental points). The figure and data are taken from ref. [22] [where the anomalous character of $I_c(x)$ was first reported] and are reproduced here for the reader's convenience.

normal modes of free $Ge(Cl, Br)_4$ molecules. Analysis along these lines has been carried out by many workers [23] and the results are shown in table 1. Of particular interest to use are the local tetrahedral modes (conventionally labelled according to their symmetries by A_1, E, F_2, F_2) whose intensities are proportional to y for $0 \leqslant y \leqslant \frac{1}{3}$ as well as an anomalous line whose intensity I_c is proportional to y^5. The strongest line is the A_1 line, corresponding to the symmetric breathing mode (Ge atom fixed) of the tetrahedron, while the second strongest line (at $y = \frac{1}{3}$) is anomalous. The frequency of this latter line is about 10% greater than that of the A_1 line for both S and Se tetrahedra (independent of the large "isotope" shift!) and we refer to its as the "companion A_1" line. The dependence on composition of $I(A_1)$ and I_c is shown [22] in fig. 7.

From fig. 7 we can conclude that the cluster responsible for the companion line contains at least five $[GeS_2(Se)_2]$ formula units (probably more, since five units are sufficient to nucleate the cluster). Because of the absence of long-range order in glasses it is natural to assume that there are many possible structures containing such a large number of atoms. Actually, however, after satisfying the constraints associated with short-range order (chemical ordering, bond lengths, chalcogen bond angles of $100° \pm 10°$, tetrahedral angles of $110° \pm 10°$) we are apt to find ourselves without any satisfactory structural models at all! Therefore the first step in constructing cluster models is to examine in detail medium-range order in networks which are known to exist at the appropriate compositions, namely the various crystalline modifications, in this case of $Ge(S, Se)_2$.

Two structurally distinct modifications are known [24] for crystalline GeS_2. The first contains $24Ge(S_{1/2})_4$ corner-sharing tetrahedra wrapped around elliptical bubbles; a Beever model * of the unit cell is shown in fig. 8. This is the low-temperature form of the material. While this three-dimensional structure does not seem to be found in g-$GeS_2(Se)_2$ it is quite interesting for several reasons. The smallest rings in the structure are Ge_3S_3 rings (puckered hexagons) similar to the 6-membered rings of the diamond structure. Rings not compounded from these units have the formula $Ge_{11}S_{11}$. In orpiment there are As_6Se_6 rings, but 12-membered rings of this type are not present in this GeS_2 structure.

The characteristic feature of the low-temperature structure shown in fig. 8 is the presence of elliptical bubbles, which can be regarded as crystalline realizations of free-volume models [25] ** of glass structures, i.e., the free volume elements have formed a superlattice (long-range order). In earlier theoretical models [25] the free (or configurational) volume ΔV was assumed to be uniformly distributed, but the more recent Cohen–Grest model of glasses ** focuses on dynamical fluctuations in

* The model shown in fig. 8 was constructed by Prof. C.A. Beevers of the University of Edinburgh.

** There is a vast difference in approach between the free-volume theories and the present work which emphasizes entropy. For example, Cohen and Grest [26] state that "the simplest [glasses] have spherical ... constituents and include the metallic glasses." The present view (see ref. [4]) is that metallic glasses represent the poorest glasses (many have been

the free volume which can be used to differentiate solid-like from liquid-like cells. The elliptical bubbles in low-T GeS_2 appear to correspond quite well to the Cohen–Grest free-volume fluctuations, although in a network structure it is not feasible to make the cellular separation they postulate.

The high-temperature crystal structure has been determined [24] in both GeS_2 and $GeSe_2$. It is a *layer* structure, with the basic units consisting of central Ge layers covered by outer chalcogen layers. Again $Ge[S_{1/2}(Se_{1/2})]_4$ tetrahedra are the basic structural units. In the (a,b) plane corner-sharing tetrahedra form chains parallel to the a-axis. In order for these chains to be cross-linked without very large distortions of bond-angles two tetrahedra *share edges* (a kind of three-dimensional analogue of diborane, H_2–B–H_2–B–H_2), as shown [27] * in fig. 9. Within the 4-ring thus formed the chalcogen bond angles are reduced from their normal value of 100° to 80°, while the Ge bond angle is reduced from 110° to 100°. These strains increase the enthalpy relative to the low-temperature form; the volume/formula unit is also increased by 2%. (The glass is 10% less dense than the crystal [28].)

To explain the stability of the layer form at high temperatures we recognize that its vibrational entropy must be greater than that of the three-dimensional form. The greatest contribution to the vibrational entropy is made by soft surface modes; the surface mode frequencies are lower than corresponding bulk frequencies. The magnitude of the reduction can be estimated from excess specific heats (e.g. $\Delta C_v/T^3$ at low temperatures T) [29,30].

For both low- and high-T forms of GeS_2 all the chalcogen atoms lie on internal surfaces. The difference between the two structures thus is quite subtle: it lies in the radius of curvature of the chalcogen-containing internal surfaces, which is infinite for the layer structure and which varies between $2d_0$ and $5d_0$ (d_0 = bond length) for the bubbles in the low-T structure. Presumably phonon softening is reduced on the curved internal surfaces. It is apparent that subtle differences on this scale lie beyond the present computational capability of molecular dynamics. This may explain the emphasis [31] on Lennard–Jones (hard-sphere) models of the glass transition; by the same token, however, Ar and other hard sphere materials are scarcely considered to be good glass-formers, so the physical significance of "glass transitions" in computer simulations of these materials remains doubtful. At best such simulations may give some description of short-range order in these unphysical "glasses", but they give no hint of the kind of medium-range order (e.g. internal surfaces) which is produced in good glass forming materials as a result of optimal

---

formed only by evaporation or splat-quenching, and have never been shown to possess glass transitions) with little or no directional character because of their large coordination numbers ($N_{cn} \gtrsim 8$) which exhaust the N_d degrees of freedom in bond-length constraints alone. Fundamental differences also exist concerning the nature of the glass transition itself in most glass-forming (i.e., polymerized) materials. I hope to examine these questions in detail in a later paper in this series.

* I am grateful to J.A. Wilson for bringing this work to my attention.

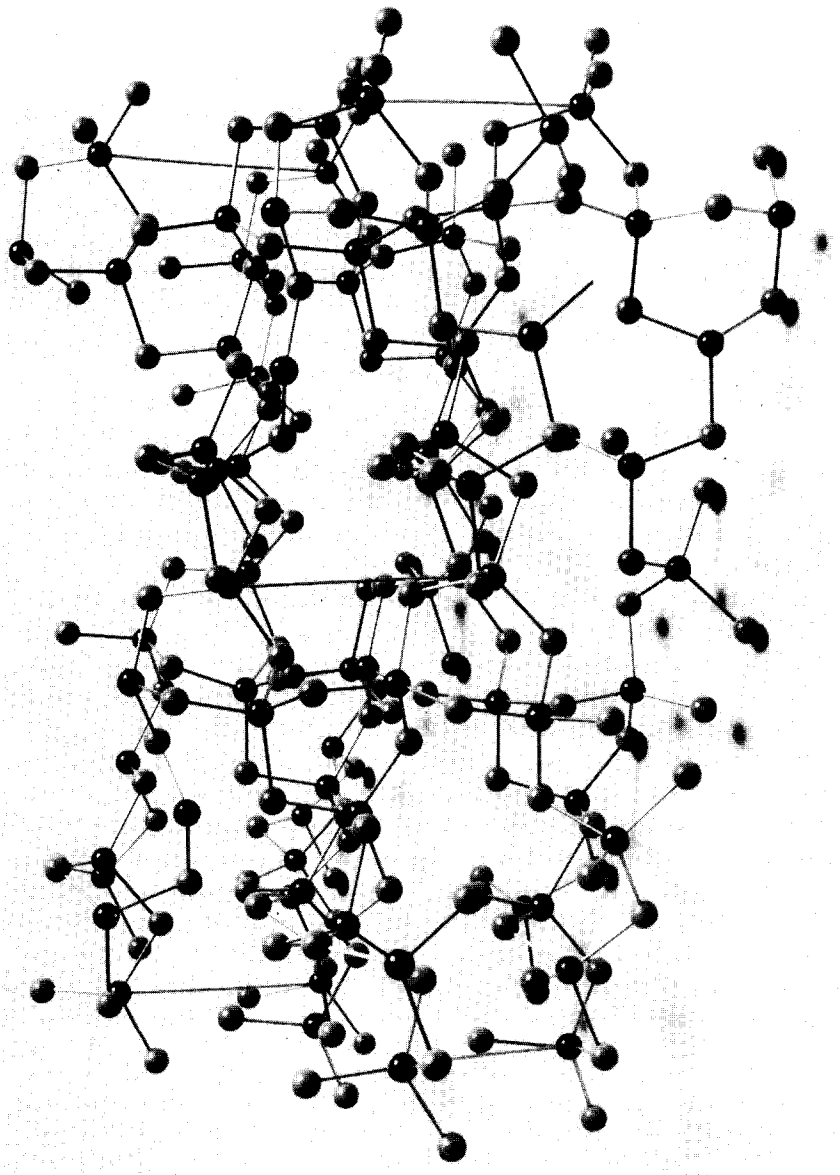

Fig. 8. Beever's miniature model of β (low temperature-) GeS_2. It is believed that this is the first explicit model of this extremely complex structure which has been constructed. The diffraction pattern has been remeasured quite recently (ref. [24]). The elliptical bubbles are supported in the model by large struts and are easily visible.

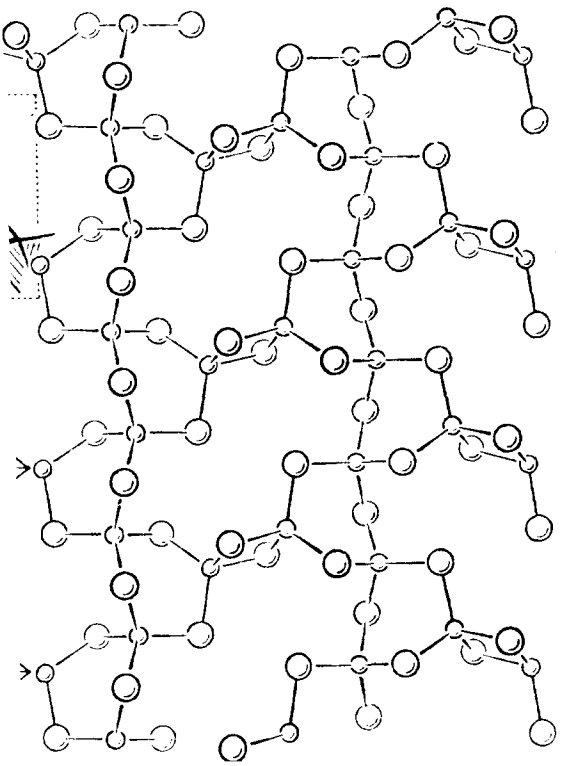

Fig. 9. The layer-crystal structure of β- (high temperature-) GeS_2. The drawing is taken from ref. [21] and is given here for the reader's convenience: it is a model drawing which shows the trilayer structure in excellent perspective.

matching of constraints and degrees of freedom [4].

That we encounter subtle differences in counterbalancing enthalpy and entropy contributions to structural dimensionality in glassy chalcogenice alloys is not surprising. Differences of this kind explain many structural transitions in crystals, and by focusing our attention on *good* glass-formers we have made such delicate balancing almost inevitable. (Comparable energy balances are encountered in many solid electrolytes; the high-temperature forms of superionic conductors such as $RbAg_4I_5$ or simply α-AgI itself can be described [32] as "entropy-stabilized.") The central question now is: which form of covalent network is "frozen-in" to g-$GeS_2(Se_2)$, the low-T (free-volume) structure, or the high-T (entropy-stabilized) layer structure?

We have seen in the previous section that the first sharp diffraction peak (FSDP) is characteristically a high-temperature anomaly associated with the interlayer spacing. However, many workers have found these data inconclusive (although the more recent data at high T in the liquid [13] are certainly compelling). What about the companion A_1 Raman peak at $\nu = \nu_c$ (table 1)? This is certainly associated

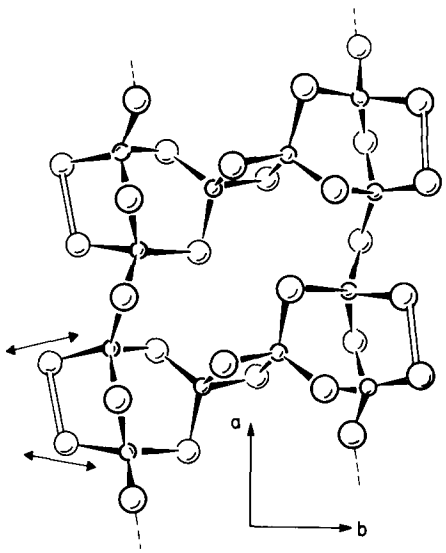

Fig. 10. Our own model for the large molecular structure responsible for the FSDP and the companion Raman line (the normal mode is shown by the arrows, corresponding to in-phase motion of dimerized edge chalcogens). The structure is called an "outrigger raft", to emphasize its edge nature, and it was first given in ref. [34].

with a large cluster, and we should be able to use it to differentiate between the two possible structures.

The layer structure readily provides a model for this peak. By terminating the unit cells in chalcogens bonded to a-axis Ge chain atoms we obtain the "outrigger raft" structure [33] shown in fig. 10, which is a fragment of the crystalline layer structure, with Ge atoms removed from the left-and-right hand edges and the neighboring chalcogens rebonded as edge dimers. Perusal of the three-dimensional geometry of the outrigger environment shows that this is possible with very little strain.

We can identify the local vibrational modes responsible for the companion line as in-phase motion of the edge dimers. Like the tetrahedral A_1 breathing mode these local modes involve motion of the chalcogen atoms primarily and so should scale with $\nu_1(A_1)$ when the chalcogen mass is changed from m_S to m_{Se} (see table 1). Because the bond vectors connecting the edge chalcogens to their respective chain Ge atoms are not quite parallel this edge motion involves a small stretching of the dimerized chalcogen bond, which could increase ν_c from ν_1 to $1.1\nu_1$. The dimerized edge chalcogens are decoupled from their environment about as well as are the tetrahedra (corner-sharing bond angle 100°, close to 90°, where the decoupling is most effective [33]). Thus the fractional line widths $\delta\nu_1/\nu_1$ and $\delta\nu_c/\nu_c$ are small (1.5%) and almost equal at room temperature [34].

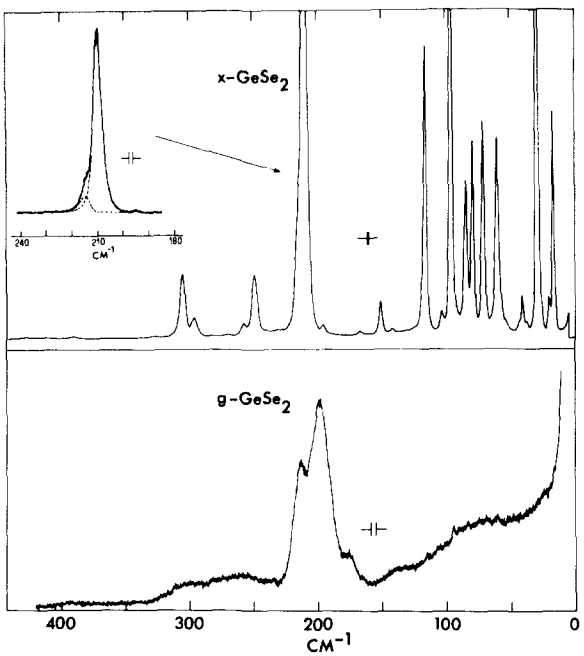

Fig. 11. Comparison of the Raman scattering spectra of c- and g-$GeSe_2$, reproduced here for the reader's convenience from ref. [34]. Of particular importance are the strong A_1 line in the crystal and the same line and its comparison, all near 200 cm^{-1}, in the glass; and the low-frequency (interlayer) modes near 17 and 30 cm^{-1}.

One of the questions that can be raised about the dimerized chalcogen-bordered raft model shown in fig. 10 is whether there is any evidence in the Raman spectrum of g-$GeSe_2$ for breakdown of perfect chemical ordering, e.g. evidence for a Se–Se stretching mode in g-Ge_ySe_{1-y} alloys which persists (albeit weakly) even at $y = \frac{1}{3}$. There actually is evidence for such a mode in fig. 11, which compares [34] the Raman spectra of c-$GeSe_2$ and g-$GeSe_2$, and in alloy data [23] on Raman scattering data from g-Ge_ySe_{1-y}. The alloy data show a Se feature (essentially Se–Se stretch in Se chains) at 250 cm^{-1} for $y = 0$ which shifts to 260 cm^{-1} for $y = \frac{1}{3}$; this small shift may be traced to the stiffening of the –Se–Se– central bond due to weakly ionic backbonds to Ge. This peak is broad and its strength is small exactly at $y = \frac{1}{3}$. The weak scattering strength is probably explicable in terms of excessive constraint near the dimerized unit. Excessive constraint makes the 215 cm^{-1} shoulder in c-$GeSe_2$ (associated with edge-sharing A_1 modes) very weak (relative strength $\frac{1}{20}$ compared to relatively unhindered corner-sharing modes, although the ratio would be $\frac{1}{2}$ if only the relative numbers of modes were important. (See inset in upper part of fig. 11.)

The isolation of a companion mode in the fragmented layer model in terms of

dimerized edge chalcogens is almost a lucky accident, corresponding to the phenomenology of the subject (i.e., this is the only such "large cluster" mode which has been identified in chalcogen alloy glasses). Can a similar device be made to work for a three-dimensional model? In view of the variation of the radius of curvature between $2d_0$ and $5d_0$ for elliptical bubbles in this model, any similar companion line should have $\delta\nu_c/\nu_c$ at least of order $(\nu_c - \nu_1)/2\nu_1 = 0.05$, which is three times larger than the observed value. Moreover, close inspection of the model shown in fig. 8 reveals that removal of a Ge atom from the three-dimensional structure followed by dimerization of the two pairs of dangling chalcogen bonds leads to interconnection of bubbles by locally planar (but otherwise anisotropically inequivalent) chalcogen-covered surfaces. It is difficult to avoid substantial inhomogeneous line broadening in this construction.

Other models for the companion A_1 line are generally unsatisfactory because they do not show how a sharp mode can be obtained from a molecular structure (e.g., a ring, see ref. [36]) which is fully embedded in a covalent network. We now turn to further evidence in the Raman-scattering spectra.

5. Very low frequency Raman lines

The room-temperature Raman-scattering spectra of crystalline and glassy $GeSe_2$ are shown [34] in fig. 11. We recognize in the glass in A_1 line near 200 cm^{-1} and its companion near 220 cm^{-1} as the strongest lines. After substraction of a light-scattering excess background [23] and deconvolution of the primary scattering a very close correspondence is recognizable between the entire spectrum of the glass and the (high-temperature) crystalline spectrum [34]. The nature of the background scattering is uncertain (it may be associated with hot carrier luminescence), but its magnitude can be greatly reduced [23] by measuring the scattering at a temperature $T \lesssim 10$ K and using longer wavelength incident radiation.

At room temperature we recognize in the crystalline spectrum in fig. 11 two strong low-frequency lines at 17 and 29 cm^{-1}. These lines are of course optic modes of the crystal, but their frequencies are much lower than those of the lowest intralayer Raman-active (E-like tetrahedral) modes which form a quartet centered near 80 cm^{-1}. We therefore infer that these modes correspond to *inter*layer modes of non-bonded sheets vibrating against each other with polarization vectors in the layer planes. From the corrugated layer geometry we can assign the 17(29) cm^{-1} lines to *a*- (*b*-) polarizations parallel (perpendicular) to the layer corrugations [34].

The Raman spectra at low frequencies are shown [23] for g-$GeSe_2$ and g-$As_2S_3(Se_3)$ in fig. 12. The characteristic behavior is $I(\nu) \propto \nu^2$ for $\nu \lesssim 5$ cm^{-1}, followed by a shoulder between 15 and 20 cm^{-1} for $GeSe_2$ and (25, 20) cm^{-1} and (30, 25) cm^{-1} for $As_2S_3(Se_3)$. Nemanich has attempted to fit this data with a theoretical model based only on acoustic modes in a *homogeneous amorphous medium* [23]; this model produces a dependence on frequency which contains terms of the

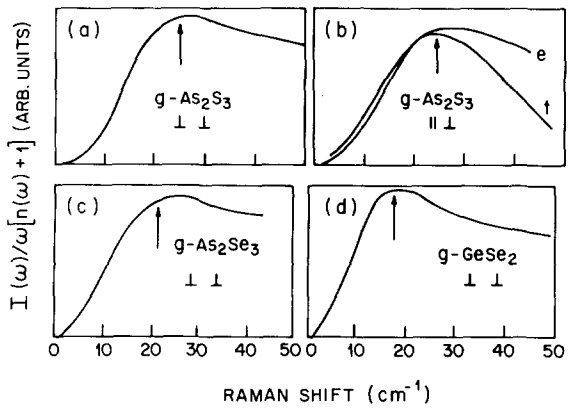

Fig. 12. Sketches of the low-frequency, low-temperature Raman-scattering spectra of $GeSe_2$ and $As_2(S, Se)_3$ (traced from ref. [23]). The arrows mark the positions of the lowest frequency (interlayer) optic phonons of the corresponding crystals. The chemical shifts are of order 50% and there is good agreement between the positions of the glassy shoulders and the lowest crystal optic photons. In (b) the experimental curve (labelled e) and a theoretical curve (labelled t) based on a disordered acoustic medium model are compared. The peak position of the theoretical curve has been adjusted to fit experiment, but there is poor agreement at high frequencies where the theoretical curve decreases too rapidly. In fact in all cases there are higher interlayer optic phonons in the crystal spectra which explain the observed experimental plateaus. These have been observed at room temperature in g-$GeSe_2$ in ref. [34] but were apparently washed out in the data shown here because of damage due to surface polishing.

form

$$I(\nu) \propto \nu^2 \exp(-\nu^2/\nu_0^2),$$

where $\nu_0 = \nu/R_0$. Here ν is a longitudinal or transverse velocity of sound (different combinations are used to explain variations of intensity with scattering polarization, but as can be seen from fig. 12 these variations are in fact small and, as Nemanich found, are not explained by the model anyway) and R_0 is the "structural correlation range." The value of R_0 is determined by the position of the shoulder and the values of ν_l or ν_t (or a weighted average). The values obtained for R_0 are of order 4 Å in $GeSe_2$.

In the layer model the basic structural units are outrigger rafts (fig. 10) which are stacked together. Note that the positions of the shoulders in the g-$GeSe_2$ scattering spectra in fig. 12 agrees quite well with the *a*-polarized interlayer optic mode at $\nu_a = 17$ cm^{-1} in c-$GeSe_2$. Similarly good agreement is obtained with the lowest frequency optic modes in c-$As_2(S, Se)_3$ marked by arrows [35]. Note that the onset of strong scattering near 17 cm^{-1} in the layer model involves optic-mode motion of large non-bonded covalent structures against one another, i.e., this frequency measures the threshold for counter-motion of internal surfaces interacting *via* van der Waals forces. This kind of motion is a form of high-frequency internal friction.

6. Outrigger rafts in $As_2(S, Se)_3$

Studies of glasses formed by alloying $GeSe_2$ with As_2Se_3 have shown [36] that the anomalous properties (such as the composition dependencies of the A_1 line and its companion) are much the same as if $GeSe_2$ had been alloyed simply with Se. The simplest explanation for this behavior is that the bordered, linearly polymerized "$GeSe_2$" rafts shown in fig. 10 form parallel bundles similar to the parallel bundles formed by linearly polymerized Se chains, and that similar chemically ordered rafts can be constructed starting from the basic ring of orpiment, c-As_2Se_3, which is an alternating (chemically ordered) As_6Se_6 unit.

The construction of orpimental outrigger rafts is by no means so straightforward as in the case of $GeSe_2$, but rafts which follow the same structural principles can be devised [37]. At first sight it appears to be possible to construct so many such rafts (composed of N = nearly 20 atoms!) that one may doubt the significance of the procedure. Actually, however, uniqueness is not the problem that it appears to be. Diffraction studies (see, e.g., I) have shown that not only is the glassy network predominantly chemically ordered, but also that the bond lengths and bond angles in g-$GeSe_2$ and g-As_2Se_3 are very close to their crystalline values. Our general theory then tells us that (slightly more or slightly less) of *all* the available degrees of freedom ($3N$) are exhausted by satisfying these constraints. If we then impose the additional conditions that we explain the FSDP, the companion Raman line, the low-frequency lines, etc., then we soon find ourselves backed into a corner where it seems that *no* model exists which will explain the data! This is why the construction of explicit models is so instructive *.

In order to construct the $GeSe_2$ raft, fig. 10, it was necessary only to remove edge Ge atoms and rebond edge chalcogens as dimers. This approach does not seem feasible for orpimental rafts, which must be constructed by removing edge As atoms and replacing them with chalcogens; this is the smallest reconstruction consistent with the basic As_6Se_6 ring structure. The latter contains several internal symmetry elements, and these must be handled carefully in order to account properly for the bond angles [37]. The way in which the enantiomorphic (left–right and up–down) symmetry evident in fig. 10 is then only partially preserved in the orpimental rafts is quite subtle. The conclusion is that there are four or five such rafts with plausible structures, compared with only one for $GeSe_2$. One of the orpimental rafts is shown in fig. 13.

The non-uniqueness of the orpimental rafts can be used to explain the anomalous temperature dependence of the position k_c of the FSDP in liquid and glassy

* In the late 1950s there were many inequivalent competing models of superconductivity. In discussing the competition, Bardeen was fond of pointing out that none of the competing models corresponded to definite wave functions: similarly here skeptics are invited to construct their own structural models which can be embedded in a space-filling network similar to chalcogenide chain bundles.

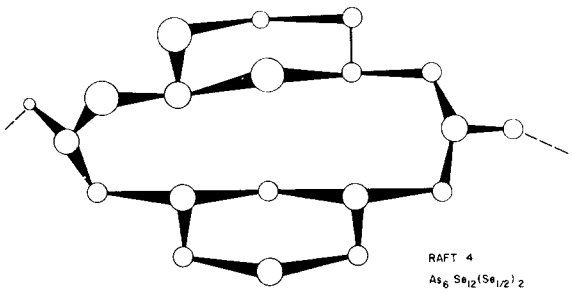

Fig. 13. An orpimental raft constructed with the same topological structure as the outrigger raft of fig. 10, viz., chalcogenide-bordered edges give rise to polymerization in one dimension and monomerization in the other two. This structure is in good agreement with diffraction, alloying and nuclear quadrupole resonance data (see ref. [37]).

As_2Se_3 (fig. 6). This is to be compared with the nearly temperature-independent k_c in $GeSe_2$ (fig. 5). The latter is expected because the "outrigger raft" conformer shown in fig. 10 is unique. With several possible orpimental conformer rafts the relative concentrations of the different rafts should change with temperature and this explains [37] the large temperature dependence of k_c in g-As_2Se_3.

A characteristic feature of orpiment is a five-layer Se–As–Se–As–se structure, compared with $GeSe_2$, which has the trilayer Se–Ge–Se structure. Electron diffraction data [38] show that the width δk_c of the FSDP is a *minimum* for $m = 1$ in $As_2Se_mTe_{2-m}$ glasses. This result is quite unexpected from the point of view of a random network model, since whatever the mechanism one invokes to explain the existence of the FSDP, random fluctuations in atomic size and bond lengths should act to increase δk_c. The observed minimum is explicable by pentalayer rafts, however, by assuming segregation of Te atoms in the outer layers. (This tendency is the one expected from the more metallic character [39] of Te compared with Se.) We also note that δk_c actually *decreases* with increasing T in liquid As_2Se_3 (fig. 6). This unexpected result may be caused [37] by the nonbonding interactions between rafts in adjacent parallel stacks; in any case the result is the opposite of what is predicted by fully bonded random network models.

After the chalcogenide-bordered orpimental rafts (such as the one shown in fig. 13) were constructed [37] nuclear quadrupole resonance data giving the distribution of the electric field gradient asymmetry parameter $\eta = Q_{zz} - (Q_{xx} + Q_{yy})/2$ at pyramidal As sits appeared [37]. These data are unexpectedly informative. In c-As_2Se_3 the As atoms are almost (but not exactly) crystallographically equivalent, and the two observed η values differ by less than 10%. If the continuous random network model of g-As_2Se_3 were correct, we would expect to observe in the glass a broad unimodal distribution of η, with its center shifted perhaps by relaxation to somewhat smaller values of pyramidal asymmetry than the crystalline value. Instead, a pronounced *bimodal* distribution has been discovered, with the two peak

values differing by nearly a factor of 3! (Shades of the "double" A_1 Raman line in g-$GeS_2(Se)_2$!) The bimodal distribution is fully compatible with the orpimental rafts, where there are two groups of As atoms (the two end atoms and the four side atoms in each bordered As_6Se_6 ring) with a population ratio of 1 : 2. The quoted weights of the two distributions of η in the glass are 4 : 6, in remarkable (and obviously unadjusted) agreement with the model.

The principal objection to chalcogenide-bordered rafts that I have encountered in discussions is that they are not perfectly chemically ordered, and that in g-$GeSe_2$ or g-As_2Se_3 the presence of even a few chalcogen–chalcogen bonds implies also the presence of a few cation–cation bonds and a small increase in enthalpy because a small part of the heat of formation of cation–chalcogen bonds [39] is thereby sacrificed. Carried to its logical conclusion this argument implies an infinite continuous covalent network which is somehow not crystalline. While many seem to feel that this problem can be resolved by invoking the magic word "random", I cannot agree. We have already seen that the VFF constraints exhaust the available degrees of freedom in As_2Se_3, and that $GeSe_2$ is actually *over*-constrained. I also find it difficult to believe that a frozen liquid can be continuously perfect with the same atomic alternation as the crystal. Reconstructed internal surfaces appear to me to be much more plausible.

Although heat of formation arguments cannot be used to justify quasi-crystalline continuity of the glassy network, they are relevant in a different way. We have seen that chalcogenide bordering can occur on any lateral scale; for example, the bilinear raft in fig. 10 could be made quadrilinear by bordering chains 1 and 4 cut out from the crystalline structure instead of chains 1 and 2. Just how large are the rafts laterally? The experimental data on η in g-As_2Se_3 suggest that the predominant rafts have the structure shown in fig. 13 with a population ratio of (bordered As)/(terminal polymerized As) of 2 : 1. However, in this case the dielectric electronegativity difference [39] between As and Se is 0.22, whereas the difference between Ge and Se in 0.44. Because the heat of formation is approximately proportional to $(\Delta X)^2$, the penalty for chalcogenide bordering should be much greater in the case of $GeSe_2$ than in the case of As_2Se_3. Thus there is a greater enthalpic inducement to lateral enlargement of $GeSe_2$ rafts than As_2Se_3 rafts.

The observed heats of formation ΔH for Ge(As)–chalcogenide bonds in crystals [39] are quite interesting. Although ΔH (Ge–chalco.) is expected to be two-four times ΔH (As–chalco.) from electronegativity differences [39], the observed values are nearly the same. This is explained by the present model on the grounds that the Ge chalcogenides are overconstrained and hence their greater ionic energy is compensated by a corresponding loss of covalent energy because of strain. This means that the strain energies, even in the crystal, are already comparable with the heat of formation and there is no compelling reason for *perfect* chemical ordering in the glasses.

7. Balanced intra- and inter-cluster forces

In section 2 we discussed topologically the influence of inter-cluster forces (also called van der Waals forces in a classical sense) on medium-range order. Similarly, in I we discussed why S and Se are good glass formers (but Te is not) from the point of view of short-range order (intra-cluster forces). In this section we bring the two approaches together more quantitatively.

The point of view taken in I was the traditional one that higher coordination numbers [Sn(6) compared with Ge(4), Te(3) compared with Se(2)] drastically facilitate crystallization. This description is not incorrect, but it does smack of begging the question. Here we take a more quantitative approach which can be used to understand the pronounced layering tendencies of chalcogenide glasses.

Our conjecture is that the marginal forces include not only the intra-cluster B–B chalcogenide interactions which produce a split B–B intra-cluster second-neighbor peak (see fig. 9 of I) but also the intercluster B–B interactions as well. Denote the former spacing by $r_B(\beta)$ and the latter by $r_B(\gamma)$. Now if $r_B(\gamma) >> r_B(\beta)$ the clusters are so far apart that only one kind of cluster is likely to be present in large concentrations, and these clusters (molecules) will readily arrange themselves to form a molecular crystal. On the other hand, if $r_B(\gamma) << r_B(\beta)$, the intercluster interactions will destroy the integroty of the clusters and again a crystal will form. (These two limits, by the way, are rather analogous to the limits $N_{cn} << 6^{1/2}$ or $>> 6^{1/2}$, as discussed in I, but now we are moving down a column (S, Se, Te) of the periodic table rather than across a row (Ge, As, Se).) The β spacing is conventionally ascribed to bond-bending valence-force field (VFF) interactions, while the γ spacing is determined by central forces between B–B nonbonded lone pairs.

In table 2 $r_B(\beta)$ and $r_B(\gamma)$ are listed for Se, Te, As_2Se_3 [10] and $GeSe_2$ [24] (layer form). The compounds have large unit cells and the quoted values represent average spacings of groups of chalcogenide pairs. The values quoted for Se and Te refer to the same crystal structure (spiral parallel chains). The results for the sulfides are very similar to the selenides.

Relative to the nearest neighbor spacing r_1 there is little difference between the Se and Te values of $r_B(\beta)$; the intrachain bond angles are 105° and 102°, respec-

Table 2
Chalcogen–chalcogen spacings (in Å) in glass-forming Se, $GeSe_2$, and As_2Se_3 compared with non-glass-forming Te

	Se	Te	$GeSe_2$	As_2Se_3
Intrachain	3.68	4.45	3.80 ± 0.2	3.78 ± 0.14
Interchain	3.46	3.50	–	3.81
Interlayer	–	–	3.85 ± 0.3	3.36, 3.95

tively. However, as the table shows, there is a large change in $r_B(\gamma)/r_B(\beta)$. Only in Se are the two values equal to within 2%; in Te the difference is 24%. Thus in glass-forming Se the intra- and inter-cluster forces are balanced, while in poorly-glass-forming Te they are not; the short intercluster-spacing in Te reflects its tendency to adopt $N_{cn} = 3$ (instead of 2) in compounds.

Is this just a coincidence? The entries in table 2 for As_2Se_3 and $GeSe_2$ show that it is not. Not only does $r_B(\beta) \simeq r_B(\gamma)$ in As_2Se_3, but the bimodal distributions of $r_B(\beta)$ and $r_B(\gamma)$ in crystalline (α) and glassy $GeSe_2$ are very similar [24]. Considering that about ten spacings each are involved in the latter examples, this is good statistical evidence in favor of the hypothesis that $r_B(\gamma)/r_B(\beta) = 1.00 \pm 0.05$ in good covalent glass formers.

Another reason for attaching glass-forming significance to the balance between intercluster and intracluster forces is that this balance is probably the mechanism which reconciles local chemical fluctuations with macroscopic chemical proportions in chalcogenide alloys. Let each (weakly polymerized) cluster be labelled as a donor (acceptor) cluster if it has more cation–cation (chalcogen–chalcogen) contacts. Thus the ethane-like cluster $Ge_2(Se_{1/2})_6$ is a donor cluster, as is As_4Se_4, while the outrigger rafts shown in figs. 10 and 13 are acceptor clusters. The topological reason for this is that completion of the connectivity (e.g., bordering of the rafts) of large clusters requires 2-fold coordinated atoms, since large clusters have well-defined surfaces.

In general the acceptor clusters are the large, stable, glass-forming units, while the donor clusters are smaller and much more deformable. This has the important consequence that the experimental signatures of the acceptor clusters are much more easily identified than those of the donors, which tend to be lost in the broad background, especially in a fully relaxed structure quenched from the melt. Thus the system will tend to appear to be acceptor-rich, even when (as in the cases of g-As_2Se_3 and g-$GeSe_2$) the numbers of donor and acceptor clusters must be equal to describe the macroscopic chemical proportions.

At first sight it may appear to the reader that this argument is a *post hoc* excuse for the fact that the stoichiometry of outrigger rafts differs from the proportions of the parent crystals which are in accord with single bonding and the $8N$ rule. However, the argument is not *post hoc* because it has been combined with the concept of balanced inter- and intra-cluster forces. We saw earlier [4] that in the good glass-forming chalcogenide alloys (Ge or As with S or Se) $T_g(x)$ parallels $T_L(x)$, whereas in the marginal glass-formers (Ge or As with Te) this was not the case. Small donor and large acceptor clusters will associate through chalcogenide–chalcogenide mediated interactions in the proper portions for electrostatic reasons and because of balance this will cost no additional energy compared with the continuous network of the crystal. In fact for S or Se (but not Te) it is the balance between inter- and intra-cluster forces that guarantees almost complete equivalence of the composition dependence of the energy of the network whether it is completely, $T_L(x)$, or only partially, $T_g(x)$ polymerized.

The strong intercluster interactions that we have been discussing are mediated by non-bonded lone-pair electrons. The valence band spectra of As, Se, As_2Se_3, etc., have the bonding electrons at low energies followed by relatively narrow bands of lone-pair electrons just below the Fermi energy. These lone pair electrons have small virtual excitation energies ΔE to antibonding conduction band states and are therefore highly polarizable (large "van der Waals" or non-bonding interactions). Increasing the lone-pair band width W_{lp} decreases $\langle(\Delta E)^{-2}\rangle^{-1}$ and therefore increases non-bonding interactions. Presumably W_{lp} is maximized when the lone-pair electrons are arranged in layers (in chemical language, the lone-pair orbitals are in resonance). This helps to explain the layering tendencies of c-As_2Se_3, c-$GeSe_2$ and a-P and As [40].

The case of a-As has been studied using several models, a three-dimensional model similar to orthorhombic c-As [41], and a warped layer model [42] containing 5-, 6-, and 7-membered puckered rings of pyramidal units. Because a-As and a-P show FSDPs and Raman scattering from a low-frequency interlayer optic phonon has been observed [40] near 40 cm^{-1} in a-P, I favor the warped layer model. If the inter-cluster and intra-cluster forces are nearly balanced, as described above, then the layer structure is quite consistent with an amorphous structure. Indeed it has been reported that sputtered a-As films can go through a glass transition upon annealing [43]. In the layer model there are $N_2 = 6$ second nearest neighbors in the layer and δN_2 second nearest neighbors in adjacent layers [40], with δN_2(a-P) = 2 and δN_2(a-As) = 4. This means that the structural differences between a-P and a-As are contained chiefly in interlayer adjustments, which are much closer for a-As than for a-P. Correspondingly the FSDP is stronger and narrower in a-P [40] than in a-As [41] indicating greater warping and incipient layer disintegration in the latter.

8. Growth kinetics and microstructure

In the next section we will discuss granular structure in amorphous Si(Ge) evaporated films. This structure has been observed directly by electron microscopy and it has a marked effect on material properties. I believe that chalcogenide glass films may also have granular structures, whether they have been prepared by evaporation or from the melt, but extensive observation of these structures by electron microscopy has not yet been reported. Later in this section circumstantial evidence for granular structure in chalcogenide films will be discussed.

We begin by discussing how microstructures may be formed kinetically. In amorphous thin films these microstructures may be columnar, and the maximum attainable thickness of the film, which eventually may tend to crack when the thickness

* These authors show that the short-range order and the ring statistics of a-As are virtually indistinguishable between the two-dimensional (layer) and three-dimensional models.

is too great, may be determined by the longitudinal stability of the columns. In bulk glasses the granular structures are probably spheroidal rather than columnar, if the temperature gradients present during quenching are small and irregularly oriented.

The traditional theory of the growth kinetics of crystals emphasizes the anisotropy of the surface energy (which is large for covalently bonded semiconductors) and the nucleation process. In the absence of impurities and boundaries the growing surfaces of the crystallite will be dominated by the most stable (and most slowly growing) surface orientation, upon which nucleation is most difficult. The nucleation problem can be relieved if the boundaries (the container) can act as a source of steps and step kinks. This is the kink-step-terrace model of crystal growth [44]. The question is: since most of the factors which dominate crystal growth are absent in the formation of non-crystalline solids, what are the principal factors determining the growth of the latter?

As I am unaware of any previous general discussion of this question, I will present my tentative ideas without the kind of rigorous support which could be provided by, e.g., molecular dynamics simulations. Some idea of the computational complexity of the problem can be obtained by noting that at present very little is known about the most primitive mathematical models of this problem, namely, Monte Carlo models of anisotropic percolation [45]. (As noted in I, the Monte Carlo models of percolation do not provide realistic descriptions of interaction energies of any kind, intra- or inter-cluster, but they are the simplest examples of network formation from separated clusters of variable size.)

Because non-crystalline materials are often prepared as thin films, we can assume a quasi-planar growth geometry for convenience. The condensing material forms islands of various areas A_n on the quasi-planar substrate. Once the spacing of these islands is smaller than the mean diffusion length l of condensing atoms on the surface, it will be energetically favorable for an atom to diffuse to the boundary of an island (which is equivalent to a step on a crystalline surface) rather than nucleate a new island. The mean diffusion length $l(T)$ is the distance an atom can diffuse on the surface before it is covered by the growth of the layer above its own layer.

At the island boundary diffusing atoms will condense or evaporate; the ratio of the two processes is determined by $\exp(-\Delta E_c/kT)$, where ΔE_c is a boundary condensation free energy. I believe that under the usual experimental conditions, which tend to maximize the substrate temperature T while still avoiding crystallization, that $\Delta E_c(n)$ may depend significantly on A_n.

Apart from the nearly constant terms associated with nearest neighbor bonding interactions $\Delta E_c(n)$ contains two competing terms, the network bond-bending strain energies and the volume energies of van der Waals attraction between non-bonding atoms. As a result of this competition some of the bond angles in clusters are displaced away from their equilibrium values, giving rise to strain energy, while the density of the non-crystalline solid ρ, is less than the crystalline density ρ_c, corresponding to a deficit in van der Waals energy. (For example, in crystalline orpiment the Se(1) and Se(2) intra-chain bond angles are close to 100°, nearly the

value in Se, which is almost strain-free because $N_{cn} = 2$ is less than $6^{1/2}$, but the Se(3) interchain bond angle has been compressed to 85° by the compacting effect of van der Waals interactions.)

The range of the bond-bending interactions is smaller than the van der Waals volume terms. Thus as A_n increases the strain energy increases harmonically (similarly to misfit energies between crystals with nearly equal lattice constants [46]). Thus $\Delta E_c(n)$ contains a term proportional to l^2, i.e. A_n itself. Moreover ρ, varies within each island, being a maximum at the center ($r = 0$) and decreasing as the limiting radius $r(n) = l$ is approached.

With crystals the anisotropy of the surface energy means that the less stable surfaces (where the barrier to nucleation is smaller) grow more rapidly, exhausting themselves as the more stable surface area increases. Analogously here there is no barrier to nucleation but with increasing A_n the growth rate decreases: island growth is self-limiting, and kinetically the islands tend to be formed with approximately equal areas.

What happens at the junction between two islands? If $N_{cn} < 6^{1/2}$, there are fewer network constraints than degrees of freedom, so that island coalescence *via* network intergrowth can take place. If $N_{cn} > 6^{1/2}$, both island networks are overconstrained and (in all likelihood) complete intergrowth would be accompanied by recrystallization. Thus in glassy Se there is no hindrance to island intergrowth and hence island or granular structure should not occur, but in a-Si(Ge) it should. In a-Si, Galeener has argued [47] that intergrowth should not occur, while Hauser has argued [48] that there is no obstacle to island network coalescence. The valence-force-field constraint theory supports Galeener's position.

As each successive layer is added to the film, the van der Waals interactions will favor centering successive islands over the centers of islands in the preceding layer; this interaction will favor columnar growth with the column axes nearly normal to the planar surface. (Even if the nucleation center of the new island does not coincide with the center of the island below it, the growth kinetics of the new island will be modifed by the van der Waals forces so that the center of the new island will migrate toward the center of the island below.) The present model assumes that the density gradient from the center of the island to its boundary is intrinsic to the amorphous structure, and so does not need to invoke temperature or concentration gradients to account for columnar formation in an "isotropic" solid *.

We now discuss experimental data on chalcogenide glasses which constitute circumstantial evidence for granular clusters and interfaces. First consider what effect the presence of rafts of $GeSe_2$-like units (fig. 10) or As_2Se_3-like units (fig. 13) will

* Metallurgical alloy ingots grown from the melt often exhibit columnar structure because of dendritic growth, favored by convection (concentration and thermal gradients), see for a summary R.D. Doherty et al. [49]. In the present situation the medium-range order (as measured by the position and width of the FSDP) scarcely varies with temperature so we turn instead to the kinetic effects produced by strain energy.

have on glasses with formulae $(As_2Se_3)_{1-x}(Se_5)_x$ or $(GeSe_2)_{1-y}(Se_3)_y$. The compound rafts tend to form stacks, as evidenced by the first sharp diffraction peak (FSDP), while the Se-rich regions are likely to consist predominantly of (quasi-cylindrical) bundles of Se chain fragments. This suggests that even though there is no long-range crystalline order, the medium-range order of the compounds is sufficiently different from that of the elements as to favor partial (quasi-stoichiometric) separation of the material. (The distances involved here can be estimated from the width of the FSDP as being of order 20–100 Å.) We will then have, in effect, granular interfaces between these quasi-stoichiometric regions. Experiments which are concerned primarily with short-range order – e.g., the diffraction spectrum apart from the FSDP – will not easily detect this incipient phase separation, however.

What are the experiments which provide indirect evidence for the existence of granular interfaces? Perhaps the most interesting are those which study the technologically promising technique called *photodoping* [50,51]. Several chalcogenide glass alloys, when rinsed in a solution containing Ag, are found to behave as lithographic masks after exposure to light and subsequent chemical fixing and development. The sensitivity of the photoresist is comparable with that of commercial polymer resists, while the resolution and some other factors are much superior. Such high sensitivity in an inorganic photoresist implies a remarkably large response of the material to the breaking of a few bonds by photons, which in turn greatly enhance Ag diffusion into the films. In all likelihood the Ag diffuses in short distances (of order a few hundred Å). Again, some quite special mechanism is required to explain why small amounts of Ag diffused into the film can so greatly alter the solubility of the exposed regions in subsequent chemical treatments. Moreover, although the structure of pure Se films is more open, this material cannot be photodoped readily.

According to our nucleation model the intergranular interface has lower mass density and higher strain energy density than the nucleation centers. Apparently c-Ag_2Se is formed in these interfacial regions during photodoping [51] but Ag diffuses readily through Ag_2Se (which is a "super-ionic" conductor), permitting the continuation of an exothermic reaction. (It seems likely that the low-density region near the interface is Se-rich, i.e., x (interface) $< x$ (average) in the Ge_xSe_{1-x} alloy, so that this reaction may be simply $2Ag + Se \rightarrow Ag_2Se$ without directly including $GeSe_2$ rafts.) In any case the channels formed by the columnar interfaces enhance the extent of Ag photodoping, and crystalization of these channels may well reduce solubility of the doped film in lithographic development.

An indirect measure of granular size is provided by the strongly enhanced far infrared absorption observed * in non-crystalline solids (including g-As_2Se_3)

* The theoretical discussion in ref. [52] (see fig. 7 especially), is based on the rather nebulous concept of "coherence length of charged defects" in an infinite continuous non-crystalline network. This concept is of doubtful significance, but it has also been used by Nemanich to

between $\omega_c = 10$ and $\omega_m = 100$ cm^{-1}. The enhancement (by an order of magnitude) is proportional to the Debye density of (acoustic mode) states and to a frequency-independent oscillator strength (in ref. 53 Glick and Yorke discussed anomalously large far infrared absorption by small metallic particles using charged surface atoms). The constant oscillator strength can arise from charged "defects" in the covalent network; of interest to us is the physical mechanism which gives rise to the lower cutoff at $\omega = \omega_c = 10$ cm^{-1}.

In the present granular model the granular diameter D is related to ω_c because the reconstructed granular surface atoms are infrared active (either because of broken bonds, or, more probably, because of breakdown of chemical ordering). When D is equal to half an acoustic vibrational wave length, adjacent grains can vibrate out of phase and interfere destrictively. (Technically speaking, the destructive interference is a dynamical local field effect.) Thus we estimate $D \simeq (\omega_1/\omega_c)\, d_c$, where ω_1 is the dominant infrared mode ($\sim$300 cm^{-1}) of a small cluster of atoms [such as $As(Se_{1/2})_3$ pyramids or $Ge(Se_{1/2})_4$ tetrahedra] of diameter d_c of order 5 Å. This gives $D = 150$ Å.

The cutoff at ω_c is sharp at $T = 300$ K. The excess low-frequency absorption at 300 K may be associated with thermal excitation of surface optic modes.

Granular vibrational properties can be studied macroscopically by measurements of acoustic attenuation and the effects of acoustic fatigue on ultrasonic sound velocities. The cohesion at granular interfaces is apparently substantially reduced by intense sound waves, which may reorient the grains and reduce the *bulk* sound velocity by as much as 20% [54]. By biasing the sample in the dark and measuring the acoustic attenuation (still in the dark) after turning off the voltage we can induce granular dipole moments. The traps which are charged in this way decay slowly (several minutes) [54] presumably by thermally induced recombination of surface traps across distances of order $D = 150$ Å.

Growth of island nucleation centers in thin films may proceed more rapidly (because the centers are more nearly strain-free) than growth in the high strain-density intergranular regions. Thus the island nuclei behave in some respects like dendrites. Recently it has been reported that substantial photo-densification can be observed in evaporated chalcogenide glass films; the magnitude of the effect is greatly enhanced when the films are prepared by beam-deposition at non-normal incidence [55]. This angular effect can be explained by columnar or dendritic shadowing, which can produce voids between dendrites; the volume of the voids increases with increasing beam declination. This effect has been simulated in mo-

describe Raman scattering (see ref. [23]) in chalcogenice glasses. Note, however,, that the infrared data on chalcogenide glasses yield $\omega_c = 10$ cm^{-1}, while the Raman data give $\omega_c = 20$ cm^{-1}! The paradox is resolved, as noted above, by recognizing that ω_c (Raman) is really an interlayer optic phonon frequency, while ω_c (infrared) does measure a distance – but it is *not* a coherence length in a continuous network; rather it is the physical granular diameter.

lecular dynamic models of crystals *, but it is surprising to encounter it in a glass, which many describe as a "random" covalent network!

The actual data for g-As_2Se_3 and g-Ge_xSe_x (maximum effect at $x = 0.25$) are [55]: contraction 0–1% for g-As_2Se_3, 0–12% for g-$Ge_{0.25}Se_{0.75}$ and 0–6% for g-$Ge_{0.33}Se_{0.67}$ (0–80° declination). Because this experiment is so novel and so successful we emphasize its importance by reproducing the composition dependence of the photocontraction in fig. 14. The trends in these extraordinarily large contractions are explicable as primarily *intrinsic* effects associated with the relative stabilities of the $GeSe_2$ and As_2Se_3 rafts.

If we compare the raft conformations (fig. 10 and fig. 13) or simply refer to the relative stabilities of q_c, with temperature (figs. 5 and 6) then we see that stable strain-free columnar growth is much more feasible with the $GeSe_2$ rafts than with the As_2Se_3 rafts. Moreover, the photocontraction data on alloys show a maximum effect at $x = 0.25$, corresponding to Se-rich intercolumnar (low density) regions. Finally, the photocontraction is *maximized* for film thickness 1.2 μ, indicating that this is the maximum columnar coherence length. The columnar nature of the obliquely deposited films is evident in SEM photographs [55].

9. Microstructure of a-Si(:H) films

Over the last decade the properties of a-Si (Ge) films have been studied by many workers, with primary emphasis on the concentration and nature of point defects. Broadly speaking, these may be divided into two classes, both of which are associated with broken bonds: reconstructed broken bonds which leave no states in the bulk energy gap, and dangling bonds, which have either singly occupied (paramagnetic acceptor) or unoccupied (empty donor) states in the bulk gap.

Because of the absence of long-range order, and because most of the point defects occur (as we shall see below) on internal surfaces, the Stokes shifts of the broken bonds are very large ($\gtrsim$0.5 eV) and very few dangling bonds are present

* In ref. [56] Dirks and Leamy reviewed the ubiquitous columnar structures often found in thin films prepared in poor vacuum and emphasized the role of low atomic mobilities in the shadowing mechanism. Even more important in most cases, in my opinion, is the role played by contaminating columnar surface layers (e.g., Al_2O_3 in the case they cite of evaporated Al films) which reinforce the columnar structure by "freezing" (i.e., differentially reducing the atomic mobility) along intercolumnar interfaces. It should be emphasized that I believe columnar growth in Ge_xSe_x alloys is much more nearly *intrinsic* in nature. Also the columnar growth in evaporated a-Si (Ge) films can occur at normal incidence and with (or without) contaminating oxides or hydrogenation. Thus while the overwhelming fraction of columnar growth (and almost all the examples discussed by Dirks and Leamy) are extrinsic and stabilized by contamination, I believe that the effects discussed here are intrinsic to large molecular clusters (in the chalcogenide case) or to proximity to the open porosity threshold [a-Si(Ge)].

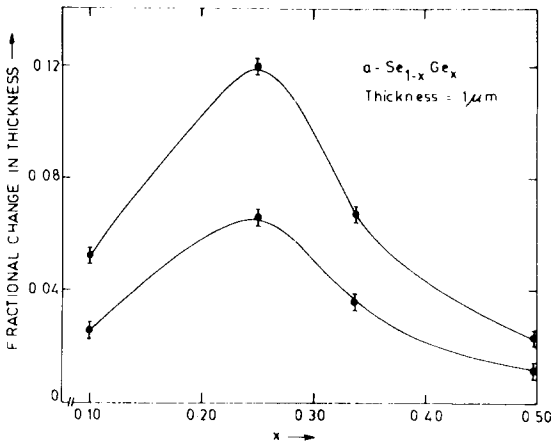

Fig. 14. Compositional dependence of photocontraction of 1 μ thick films with angles of incidence for beam deposition of 60° (lower curve) and 80° (upper curve). These data (from ref. [55]) probably represent the first evidence for intrinsic dendritic shadowing in non-crystalline films.

compared to the total number of broken bonds. (Speaking simply, one can say that it is energetically favorable for the structure to reconstruct in such a way as to eject broken bond states from the energy gap [57]. However, as obvious as this idea is, confirming it in explicit model calculations may not be so easy, because we must find the correct relaxation of the configurational coordinates to obtain simultaneously complete ejection of both occupied acceptor-like and unoccupied donor-like states from the energy gap. In the very simplest case, the (110) natural cleavage surface of GaAs, this has been achieved only quite recently by combining elaborate LEED experiments and self-consistent pseudopotential calculations [58]. Within the context of schematic model Hamiltonians, on the other hand, we are likely not only to get the individual energy levels wrong, but we can even obtain unphysical results [59] which predict, for example, that the natural cleavage surface of Si is (100) instead of (111)! Thus the results from over-simplified models can be so poor as to render hopeless the task of understanding the main physical effects. In what follows we attempt to avoid these problems by relying on well-established results for point defects on crystal surfaces and general topological arguments to analyze the experimental data on amorphous semiconductor films.)

Perhaps the most puzzling anomaly is the experimental observation that the minimal conconcentration of paramagnetic bonds (denoted by c_0) is generally of order $(1 \pm 0.5) \times 10^{-3}$, while the minimal concentration x_0 of broken bonds (as determined, e.g., by hydrogenation [60] or density deficit [61] measurements) is of order $(1 \pm 0.5) \times 3.5 \times 10^{-2}$. If c_0 were of the order of $(0.1-0.2)x_0$, this would be explicable in terms of the large Stokes shifts customarily found with broken bonds at point defects (such as vacancies) in crystals. Or if c_0 were less than 10^{-6} (as in an annealed chalcogenide glass film) then we could argue that the relaxation is

essentially completely effective in non-crystalline solids, but this description does not apply to a-Si (Ge) films either.

I have suggested previously [62] a topological solution to this awkward problem, but before we discuss the topological solution let us consider an explanation put forward by experimentalists who have studied the density deficit [61]. They argue that the density deficit (of amorphous relative to crystalline material) is concentrated in microvoids, and that these microvoids contain, say, 20 or so broken bonds; these bonds are paired, so that if their number is even there are no dangling bonds associated with the void, but if their number is odd, there is a dangling bond.

This argument, if valid, explains the data. However, the argument has a *post hoc* character. It has been shown [63] by analyzing photoemission data that a-Si films (at least within the photoelectron escape depth, 10–20 Å of the surface) contain a large density of 5- and 7-membered rings. Associated with each surface 5- and 7-membered ring there is probably a dangling bond. This argument, based on ring statistics, is a more logical way of formulating the even–odd mechanism, but it predicts too large a value of c_0 (of order $0.1–0.2\, x_0$).

A more general topological argument can be made, based on growth kinetics, which is more physical and less arbitrary. Evaporated films grow by nucleating islands which expand laterally until they approach within a van der Waals radius of another island. Can two such islands coalesce? The answer depends on the number of valence force-field constraints, N_{con}, compared with the number of degrees of freedom per atom. N_d, or on whether the mean coordination number $m \gtrless m_c = 6^{1/2}$ (see I). If $N_{con} >> N_d$, then complete coalescence or island intergrowth would require too much strain energy, while if $N_{con} < N_d$ no strain energy is required and islands should not form. The interfaces between islands can be described as grain boundaries because there is a density deficit in their neighborhood just as there are density deficits in the cores of arrays of dislocations, which can be used to describe grain boundaries between crystalline material.

When crystallites grow, the surface area of the crystallite is dominated by orientations with the lowest surface energy [e.g., (111) for Si(Ge), (110) for zinc blende crystals such as GaAs] which are also the natural cleavage faces of the crystal. In an amorphous island with $N_{con} >> N_d$ locally the island surface will still resemble the crystalline surface of lowest energy. As the two amorphous grains come almost into contact, the harmonic strain energy required to produce complete intergrowth is of the order of $2(N_{con} - N_d)\, kT_m/3$ per atom, where T_m is the melting point (since $T_g \simeq 2T_m/3$; see discussion in I of equipartition of strain energies). With $N_{cn} = 4$ this is of order 0.1 eV/atom, whereas the estimated crystalline surface energy per atom (after reconstruction) may be of order * 0.6 eV/atom. I assume

* Monovacancy formation energies are about 2.0 eV/4 broken bonds [64], but a large part of this formation energy is "metallic" in character, so that the surface energy of an atom with one broken bond is larger than 0.5 eV. On the other hand, the reconstructive recovery or reduction of formation energies is expected to be more complete on an internal surface of an amorphous material where strengthening the back bonds produces smaller strains in the second neighbor bonds. See also ref. [65].

that the anharmonic strain energy is large anough ($\gtrsim$0.5 eV) to cause the total strain energy to exceed amorphous surface strain energy, because of the columnar microstructure observed by electron microscopy [48,66].

On a granular surface reconstruction should take place much as it does on the analogous crystal surface, e.g., on Si(111) where there is one broken bond/surface atom, the cleaved surface reconstructs in a 2×1 pattern which leaves no dangling bonds/surface atom [62]. However, the convexity of the granular surface may be distributed abruptly enough to produce identifiable lines of edge atoms, with, again in the case $N_{cn} = 4$, two broken bonds/surface atom, which after reconstruction leaves one dangling bond/surface atom [62]. (In general, the effect of reconstruction is to reduce the number of dangling bonds/atom to one less than the number of broken bonds/atom. This is the case for c-Si and Ge, unless very elaborate reconstruction patterns (large unit cells) are invoked. I assume that such elaborate reconstruction is not feasible on an amorphous surface.)

With this extensive background based on experience with broken bonds on crystalline semiconductor surfaces one can now calculate (to within a factor of order unity) that [62]

$$c_0 = x_0^2,$$

a relation which is very well satisfied by $x_0 = 3.5 \times 10^{-2}$ and $c_0 = 10^{-3}$, the experimental values [60]. This discussion shows that internal surfaces in general and the microstructure produced by a specific preparative procedure determine the defects in amorphous networks, and that these should not be regarded as being "randomly" or homogeneously distributed in the material. However, microstructural trends connected with arrays of defects on internal surfaces can be obscured by gettering of impurities (such as oxygen) during deposition, so that the characterization of the connection between defect properties and microstructure requires carefully controlled experiments.

Knights et al. have recognized [66] that microstructural dimensions (e.g., columnar diameters and grain-boundary widths) can be varied systematically during plasma hydrogenation, and have shown that there exist very strong correlations between microstructural morphology (as revealed by electron microscopy) and point-defect properties (such as the relative concentrations of SiH and SiH_2 units). The question of the nature of the grain boundary regions [which are also observed [48] as columnar interfaces in evaporated or sputtered a-Si (Ge) without H] is at present unresolved and will now be discussed from the viewpoint of VFF constraint theory.

The central problem here is the *width* of the grain-boundary (intercolumnar) walls. In a-Si : H_x films this width may vary with x, both because the walls are H-rich and because the strain-relieving (softness) demands on the network depend on whether the dominant unit is SiH [as in an hydrogenated C-Si (111) surface] or is SiH_2 [which can form polymerized $(SiH_2)_n$ chains]. It would seem that further insight into these problems will be obtained when the data of Knights et al. [66]

are combined with the results of kinetic studies [67] of a-Si : H obtained from-c-Si by implantation of Si and H.

The problem of the width of the grain-boundary walls is more obviously intrinsic in the case of a-Si (Ge) films, which exhibit the same kind of columnar structure (similar center-to-center spacings and wall widths of order several 10^2 Å) as a-Si : H_x films. If a-Si (Ge) were to consist only of islands of homogeneous "random" networks, then the wall width would be of order $d = 4$ Å (a second-neighbor spacing in the network), whereas the observed [48] wall widths are of order 30 times larger, i.e., of order d/x_0 (x_0 = concentration of broken bonds).

This situation, in which there may be an intrinsic surface/volume ratio (assuming, for example, that most of the broken bonds occur in quasi-planar arrays) is highly reminiscent of percolative models near the connectivity thresold. Ordinarily the connectivity threshold refers to atom (bond) connectivity; here, we mean, of course, vacancy or void connectivity, which we call the open porosity threshold. In both cases the connectivity refers to a micronetwork, and the critical density at which the network is barely connected is associated with a characteristic surface/volume ratio [68].

If the system were in equilibrium, then near the critical density all dimensions associated with density fluctuations become very large (analogously to critical opalescence). Non-crystalline films are, of course, not in equilibrium, but experience has shown that the concentration of point defects in evaporated a-Si can be minimized, e.g. by deposition on substrates heated to the maximum temperature compatible with non-crystallization. This annealing process may, in effect, bring the system closer to equilibrium. The question then remains, why should the density be such that the material is close to the open porosity threshold? Wouldn't this be a rather improbable accident?

When $N_{con} >> N_d$ we have seen that even a non-crystalline network is under strain, that this strain energy probably increases [46] like R^2 (where R is the distance to the center of an island, column, or spheroidal grain), that the increasing strain energy slows radial growth, and that island intergrowth or coalescence becomes unlikely. When the local strain energy is large, it is energetically favorable to have connected internal surface (open porosity) near the granular surface, because this permits the reduction of the strain energy by surface diffusion of the atoms as they are deposited. This effect tends to reduce the density below ρ_{op}, the density associated with the open porosity threshold. At the same time the van der Waals forces between non-bonded atoms inhibit the formation of wide voids and act to increase the density so that it falls *just below* (rather than far below) ρ_{op}. Thus the proximity of the evaporated material to the open porosity threshold is not accidental; in fact, it is almost inevitable, providing that the material is not contaminated so much as to inhibit surface diffusion by segregation of the impurities on the internal surfaces.

By the same token the kinetics of island growth in an overconstrained network near the open porosity threshold probably imply that $\rho > \rho_{op}$ near the island cen-

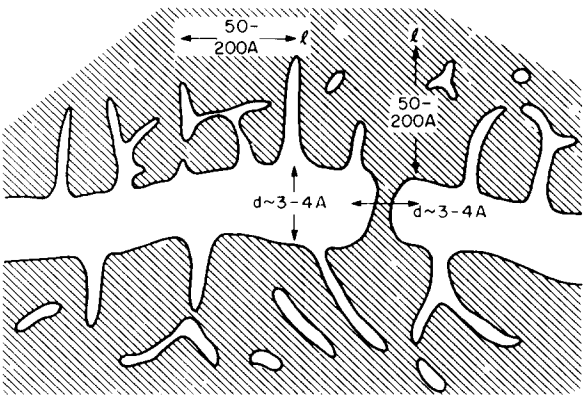

Fig. 15. The open porosity or fenestration of the interface between amorphous islands which arises because of proximity to the open porosity percolation threshold. Although the two islands approach within a van der Waals radius (~4 A) of one another, there is a low-density (fenestrated) region of order a surface diffusion length (i.e., of order 100 A near room temperature) in depth on both sides of the interface.

ter, $0 \leqslant R < R_1$, while $\rho < \rho_{op}$ for $R_1 < R < R_{max}$. In the latter region the material is fenestrated, i.e., permeated by a void network, as shown in fig. 15. This is the low-density region observed by electron microscopy [48].

What can be said about R/R_{max}, i.e., the relative filling factor for the porous regions? We woulx expect that the fenestration filling factor $(R_{max} - R_1)/R_{max}$ would increase with $(N_{cons} - N_d)/N_d$, i.e., reach its maximum in a-Si and vanish in g-As_2Se_3. (Actually because of the presence of van der Waals forces $(R_{max} - R_1)/R_{max} > 0$ even in g-As_2Se_3, as shown by photocontraction experiments [55]. However, in g-Se probably $R_1 = 0$ and complete coalescence occurs, with no columnar structure.) As we have noted previously, R_{max} itself depends primarily on the surface diffusion length, which may be roughly independent of composition for deposition temperatures just below the recrystallization temperature. Thus, experiments on the composition dependence of R_1/R_{max} would be of great interest, as suggested by Hauser [69].

The densities ρ_e and ρ_b of evaporated and ion-bombarded (previously crystalline) films are expected to bracket the open-porosity density threshold ρ_{op}, i.e., $\rho_e \lesssim \rho_{op} < \rho_b$. Recent ellipsometric neasurements [70] on Ge films have $\rho_e/\rho_c = 0.87$, $\rho_b/\rho_c = 0.93$, which leads me to guess that $\rho_{op}/\rho_c = 0.89 \pm 0.02$ in terms of ρ_c, the crystalline density. The van der Waals forces are relatively weaker, and the reconstructive covalent forces relatively stronger, in Si compared with Ge, so that the internal surfaces are more stable; this means that ρ_{op}/ρ_c in a-Si should be larger than in a–Ge; a plausible guess is $\rho_{op}/\rho_c = 0.93 \pm 0.04$ for a-Si.

Direct evidence of proximity to the open porosity threshold of a-Si films was obtained [71] when the films were deposited at 350°C in ultra-high vacuum ($<10^{-8}$

Torr) and the dangling bonds were successfully quenched by plasma hydrogenation in the range 500–550°C. (The films recrystallize above $T_R = 600$°C.) This experiment clearly demonstrates the connectivity of the microvoid network. Recently even more persuasive evidence which demonstrates a qualitative difference in topology between evaporated and ion-bombarded (previously crystalline) films has been obtained through studies of crystalline regrowth kinetics [72]. The intrinsic regrowth rates are much (an order of magnitude or more) greater in the evaporated case. According to the ideas we have discussed, the most likely explanation for this behavior is that the void surfaces are largely connected in the evaporated material, $\rho_e < \rho_{op}$, and are largely isolated in the ion-bombarded material, $p_b > \rho_{op}$. Then during regrowth the growth front envelopes the isolated microvoids but is arrested by the extensively interconnected internal surfaces. This experiment not only supports our ideas but it also demonstrates their explicit operational significance and predictive character [62] which is important because many scientists are inclined to attach greater significance to point-defect than to extensive properties.

When UHV films are deposited at 350°C the effect of exposure to air on the dangling bond structure was found to be negigible for nomal 0° deposition but the paramagnetic spin density decreased by a factor of 2.2 for 60° deposition [73]. Again this can be explained by dendritic growth and void generation by shadowing. Subsequent oxidation may quench the paramagnetic spin density of the more porous 60° film. Presumably when the 0° films are exposed to air the thin(~10–20 Å) surface oxide that forms seals off the network from further oxidation. This would be expected if the film density ρ was slightly below ρ_{op}. The restrictions on vacuum conditions reported as necessary for post-deposition [71] hydrogenation are similar to those required for rapid recrystallization [72].

The present analysis is consistent with the most recent discussion of growth morphology of plasma-deposited a-Si : H films given by Knights [66]. He concludes that changes in deposition parameters other than temperature affect the degree of coalescence of the islands (the fenestration factor $(R_{max} - R_1)/R_{max}$ more than the island spacing R_{max}. Presumbaly R_{max} depends on the mobility of the most mobile surface species while R_1 depends on the degree to which hydrogenation relieves the network strain. Formation of $(SiH_2)_n$ polymers may fill the fenestrated region without relieving the strain (small R_1). Formation of SiH units may relieve the strain associated with broken bonds on quasi-(1 1 1) internal surfaces. Thus the deposition conditions which favor the formation of SiH units compared with $(SiH_2)_n$ polymers produce a lower defect density and may reduce the volumes of the fenestrated regions below the minimum observable by electron microscopy.

As noted by Knights, a-Si(:H) films possess considerable internal stresses similar to polycrystalline films, and microscopically these latter stresses are often described in terms of lattice parameter variations. This is the macroscopic aspect of the VFF constraint model introduced in I. The strength of our present topological approach is that we have been able to identify chemical trends in non-local strain energies without having available to us the convenient reference frame of a lattice.

The effects of constraints and kinetics on density fluctuations can be examined with high resolution electron microscopy [48,66,69]. The composition dependence of these fluctuations should be strongly influenced by the strain energy. In I we discussed strain energy primarily from the point of view of covalent (bond bending) forces, whereas in this paper we have seen many illustrations of the importance of van der Waals forces. The qualitative effect of the latter is illustrated in fig. 16 for the virtual atom model (average coordination numbers in an isotropic network; the corrections associated with integer coordination and anisotropy, e.g., rafts, should be small). The abrupt discontinuities in dX/dm, i.e., the derivatives of the configurational strain enthalpy ($X = \Delta Hs$) or configurational entropy ($X = \Delta S$) which must occur at $m = m_c$ when $N_{con} = N_c$ in a self-contained model based only on VFF, are removed when the effects of van der Waals dorces are included.

From fig. 16 and from figs. 1–3 it is also evident that $m = 2$ may be especially significant. I have assumed, in drawing fig. 6, that $\Delta H(m \leqslant 2) = 0$, and that ΔH is proportional to $(m-2)^a$ for $2 \leqslant m \leqslant m_c$ with $a \geqslant 2$. The justification for this assumption is that the initial effect of branching should be described by pairing (fig. 3).

Coalescence of islands is inhibited by a non-adiabatic (dynamical) energy barrier during solidification from the vapor or the melt. The dynamic effects are probably much larger in vapor deposition than in melt quenching, and it may be reasonable to assume that the coalescence energy barrier ΔU is proportional to $\Delta H - \tilde{T}\Delta S$ where $\tilde{T}$ is close to T_g for melt quenching and to T_s (the substrate temperature) for vapor deposition. Typically $T_s \simeq T_g/2$, so that for vapor deposition ΔU is larger than for melt quenching, which favors granular formation in evaporated materials.

For g-As_2Se_3 we guess that $\Delta U \simeq \Delta H_s - T_s\Delta S \simeq 3kT_g$ and these guesses have

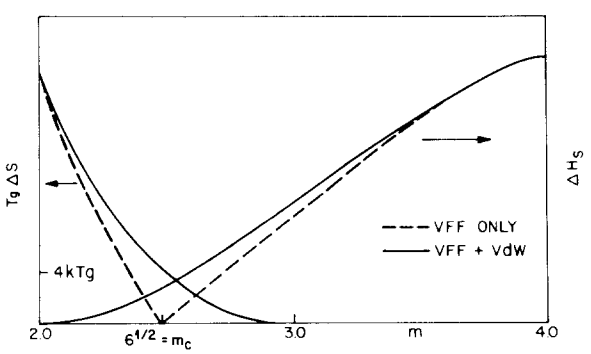

Fig. 16. Topological trends in configurational strain enthalpy (ΔH_S) and entropy (ΔS) as a function of m in the virtual atom model. Because of clustering effect the behavior of actual amorphous and glassy covalent solids will differ somewhat from the predictions of this model, but the broad trends should be described correctly. Note that ΔH_S describes only the strain enthalpy associated with intercluster intergrowth, not the complete configurational enthalpy ΔH, which must always satisfy the condition $\Delta H(T) \geqslant T\Delta S$ for $T \geqslant T_0$.

been used to indicate a very crude energy scale in fig. 16. This is, of course, only a schematic expedient, but until accurate thermodynamic and kinetic data are available this sketch may at least be useful as a qualitative guide to chemical trends in island coalescence.

Some very recent data [74] on the microstructure of ion-implanted InSb surfaces are of interest because the electron micrographs suggest that the fenestrated (or spongy) microstructures which are found in evaporated semiconductor films can be produced by ion bombardment near the *free* surface of a crystalline semiconductor. The sponginess (depth of fenestrated region) is maximized for InSb when the ions are As^+, Sb^+ or Bi^+. The first two may simply replace native Sb atoms which are "boiled off" during implantation; this process is the inverse of evaporative deposition and so spongy material ($\rho < \rho_{op}$) is produced. It is most interesting that Bi^+ can also be used as effectively as Sb^+. This apparently implies that the Bi is replacing Sb on the four-fold coordinated sites of the fenestrated region, i.e., locally amorphous InBi is being synthesized, although crystalline InBi has the tetragonal PbO structure and is metallic. The energy gap in a-Si is about twice as large as in c-Si, so a-InBi could be a semiconductor and could have a structure similar to a-InSb.

10. Conclusions

In I and this paper we have explored short-range and medium-range order in glassy and amorphous semiconductors. Our aim has been to identify the broad trends in structural behavior from Se($N_{cn} = 2$) to Si($N_{cn} = 4$) and to correlate these with material properties. We have seen that generally for $m \leqslant 2.5$ configurational entropy plays a dominant role and that for $m \geqslant 3$ configurational strain energy is usually dominant. We have seen that specific models of the networks can be constructed which allow for the combinational character of the structure. The effect of kinetics on microstructure has been discussed in topological terms, and the entire discussion has been carried out in the context of a wide range of carefully selected data.

The reader whose patience and perseverence have carried him thus far in these two rather lengthy papers may wish to pause at this point and compare the microscopic pictures of the atomic structure presented at the end of I (figs. 11 and 12) with figs. 10 and 13 of the present paper. This comparison illustrates the progress that has been made in understanding the structural nature of covalent non-crystalline semiconductors. The nearly random, fully three-dimensional models shown in figs. 11 and 12 of I were derived from analysis of diffraction data alone. The layer structures of the present figs. 10 and 13 are based not only on the short-range order described by the diffraction data, but also on the medium-range order implied by thermochemical and Raman data. By combining all these data we can establish the dimensionality of the polymerized chalcogenide glass structures. This is summarized

Table 3
Dimensional regression in the compound chalcogenide glasses

N(poly)	As_2Se_3	T	$GeSe_2$
0	Normal liquid (monomerized, stacked rafts)	↑ T_m	Normal liquid (monomerized stacked rafts)
1	Glass (linearly polymerized stacked rafts)	↑ T_g	Glass (bilinearly polymerized stacked rafts)
2	Crystal (planar-polymerized chains)	↑	Crystal (α) (planar-polymerized corner-and-edge-sharing tetrahedra)
3	(Sb_2Se_3 structure splintered orpiment)		Crystal (β) (corner-sharing tetrahedra: "free-volume" bubbles)

for the reader's convenience in table 3, which shows the trends in dimensionality of the local polymerization texture from low temperatures (most stable crystal structure) to high temperature (normal liquid or gas).

The structural models described here and in I can be used to discuss the kinetic nature of the glass transition. This subject will be explored in III of this series. It should be evident from the structural emphasis of my presentation, from the importance of entropy and combinatorial requirements, and from the attention paid to non-local (granular, columnar, and more generally, internal surface) properties that I do not attach much significance to theoretical treatments of this subject based on random covalent networks or schematic model Hamiltonians in which neither the roles play by constraints nor the physically significant coordinates are discussed.

I an grateful to J.C. Knights, R.J. Nemanich, P.C. Taylor and R. Zallen for preprints and discussion.

References

[1] R.O. Davies and G.O. Jones, Adv. Phys. 2 (1953) 370.
[2] W. Kauzmann, Chem. Revs. 43 (1948) 43; M. Fixman, J. Chem. Phys. 69 (1978) 1527; 1538.
[3] A.A. Miller, Macromol. 3 (1970) 674; C.A. Angel and J.C. Tucker, J. Phys. Chem. 78 (1974) 278; C.A. Angell and W. Sichina, Ann. N.Y. Acad. Sci. 279 (1976) 53; A.J. Easteal, J.A. Wilder, R.K. Mohr and S.T. Moynihan, J. Am. Ceram. Soc. 60 (1977) 134.
[4] J.C. Phillips, J. Non-Crystalline Solids 34 (1979) 153.

[5] M.R. Hoare and J.A. Barker, Structure of Non-Crystalline Materials, ed. P.H. Gaskell (Taylor and Francis, London, 1977) p. 173; M.R. Hoare, J. Non-Crystalline Solids 31 (1978) 157.
[6] G.A.N. Connell and G. Lucovsky, J. Non-Crystalline Solids 31 (1978) 123; A. Feltz and L. Senf, Z. Anorg. Allg. Chem. 444 (1978) 195.
[7] D. Beeman and R. Alben, Adv. Phys. 26 (1977) 339.
[8] J. Bornarel, J. Appl. Phys. 43 (1972) 845.
[9] A.A. Vaipolin and E.A. Porai-Koshits, Sov. Phys.–Solid S. 5 (1963) 186.
[10] A.L. Renninger and B,C. Averbach, Phys. Rev. 8B (1973) 1507.
[11] A.J. Apling, A.J. Leadbetter and A.C. Wright, J. Non-Crystalline Solids 23 (1977) 369.
[12] L. Cervinka and A. Hruby, in: Amorphous and Liquid Semiconductors, eds. J. Stuke and W. Brenig (Taylor and Francis, London, 1974) p. 431.
[13] O. Uemura, Y Sagara, D. Muno and T. Satow, J. Non-Crystalline Solids 30 (1978) 155.
[14] J.S. Lannin and B.V. Shanabrook, Sol. St. Commun. 28 (1978) 497.
[15] R.J. Nemanich, G.A.N. Connell, T.M. Hayes and R.A. Street, Phys. Rev. 18B (1978) 6900.
[16] O. Uemura, Y. Sagara and T. Satow, Phys. Stat. Sol. A26 (1974) 99; O. Uemura, Y. Sagara, M. Tsushima, T. Kamikawa and T. Satow, J. Non-Crystalline Solids 33 (1979) 71.
[17] G.A.N. Connell and R.J. Nemanich, private communication.
[18] D.J. Sarrach, J.P. DeNeufville and W.L. Haworth, J. Non-Crystalline Solids 22 (1976) 245.
[19] M.B. Myers and E.J. Felty, Mat. Res. Bull. 2 (1967) 535.
[20] A.J. Leadbetter and A.C. Wright, J. Non-Crystalline Solids 7 (1972) 23.
[21] J.C. Phillips, Ferroelectrics 16 (1977) 3, Electrochimica Acta 22 (1977) 709.
[22] P. Tronc, M. Bensoussan, A. Brenac and C. Sebenne, Phys. Rev. B8 (1973) 5947.
[23] R.J. Nemanich, Phys. Rev. B16 (1977) 1655; N. Kumagai, J. Shirafuji and Y. Inuishi, J. Phys. Soc. Jap. 42 (1977) 1262; G.J. Ball and J.M. Chamberlain, J. Non-Crystalline Solids 29 (1978) 239.
[24] G. Dittmar and H. Schafer, Acta Cryst. B32 (1976) 1188; 2726.
[25] M.H. Cohen and D. Turnbull, J. Chem. Phys. 31 (1959) 1164.
[26] M.H. Cohen and G.S. Grest, Phys. Rev. Lett. 45 (1980) 1271.
[27] F. Hulliger, Structural Chemistry of Layer-Type Phase, ed., F. Levy (Reidel, Boston, (1976).
[28] R. Azoulay, H. Thibierge and A. Brenac, J. Non-Crystalline Solids 18 (1975) 33.
[29] T. Ninomiya, J. Phys. Soc. Jap. 44 (1978) 263; 269.
[30] R.B. Stephens, Phys. Rev. B8 (1973) 2896.
[31] H.R. Wendt and F.F. Abraham, Phys. Rev. Lett. 41 (1978) 1244.
[32] J.C. Phillips, J. Electrochem. Soc. 123 (1976) 934.
[33] P.N. Sen and M.F. Thorpe, Phys. Rev. B15 (1977) 4030.
[34] P.M. Bridenbaugh, G.P. Espinosa, J.E. Griffiths, J.C. Phillips and J.P. Remeika, Phys. Rev. B20 (1979) 4140.
[35] R. Zallen, M.L. Slade and A.T. Ward, Phys. Rev 3B (1971) 4257; R. Zallen and M.Slade, Phys. Rev. 9B (1974) 1627.
[36] R.J. Nemanich and S.A. Solin, Sol. St. Commun. 21 (1977) 273.
[37] J.C. Phillips, C.A. Beevers and S.A.B. Gould, Phys. Rev. 21B (1980) 5724.
[38] J. Chang and R.B. Dove, J. Non-Crystalline Solids 16 (1974) 72.
[39] J.C. Phillips, Bonds and Bands in Semiconductors (Academic , New York, 1973) p. 93; R.A. Street and G. Lucovsky, Sol. St. Commun. 31 (1979) 289.
[40] J.S. Lannin, Sol. St. Commun. 25 (1978) 363; J.S. Lannin and B.V. Shanabrook, Sol. St. Commun. 28 (1978) 497.
[41] G.N. Greaves, S.R. Elliott and E.A. Davis, Adv. Phys. 28 (1979) 49.
[42] D. Beeman and R. Alben, Proc. 7th Int. Conf. Amorp. and Liquid Semicond. Univ. of Edinburg, 1977).

[43] J.P. De Neufville, Proc. 5th Int. Conf. on Amor. and Liquid Semicond (Taylor and Francis, London, 1973) p. 419.
[44] H.C. Abbink, R.M. Broudy and G.P. McCarthy, J. Appl. Phys. 39 (1968) 4673; M. Shimbo, J. Nishizawa and T. Terasaki, J. Cryst. Growth 23 (1974) 267.
[45] L. Turban, J. Phys. C 12 (1979) 1479.
[46] F.C. Frank and J.H. van der Merwe, Proc. Roy. Soc. London A 198 (1949) 216.
[47] F.L. Galeener, Phys. Rev. Lett. 27 (1971) 421.
[48] J.J. Hauser, Phys. Rev 8B (1973) 3817.
[49] R.D. Doharty, P.O. Cooper, M.H. Bradbury and F.J. Honey, Met. Trans. 8A (1977) 297.
[50] A. Yosikawa, O. Ochi, H. Nagai and Y. Mizushima, Appl. Phys. Lett. 31 (1977) 161.
[51] C.H. Chen and K.L. Tai, Appl. Phys. Lett. 37 (1980) 605.
[52] U. Strom and P.C. Taylor, Phys. Rev. 16B (1977) 5512.
[53] A.J. Flick and E.D. Yorke, Phys. Rev. 18B (1978) 2490.
[54] S. Okano, H. Nagaoka, M. Suzuki and T. Hata, Sol. St. Commun. 28 (1978) 369; T.N. Claytor and R.J. Sladek, Phys. Rev. Lett. 42 (1979) 1482.
[55] B. Singh, S. Rajagopalan, P.K. Bhat, D.K. Panhys and K.L. Chopra, Sol. St. Commun. 29 (1979) 167; J. Non-Crystalline Solids 36 (1980) 1053.
[56] A.G. Dirks and H.J. Leamy, Thin Solid Films 47 (1977) 219.
[57] J.C. Phillips, Comm. Sol. St. Phys. 3 (1970) 105.
[58] J.R. Chelikowsky and M.L. Cohen, Sol. St. Comm. 29 (1979) 267; Phys. Rev. B20 (1979) 4150.
[59] D. Adler, Phys. Rev. Lett. 41 (1978) 1755.
[60] P.A. Thomas, M.H. Brodsky, D. Kaplan and D. Lepine, Phys. Rev. 1318 (1978) 3059; D. Kaplan, N. Sol and G. Velasco, Appl. Phys. Lett. 33 (1978) 440.
[61] R.J. Temkin, W. Paul and G.A.N. Connell, Adv. Phys. 22 (1973) 581.
[62] J.C. Phillips, Phys. Rev. Lett. 42 (1979) 1151.
[63] J.D. Joannopoulous and F. Yndurain, Phys. Rev. B10 (1974) 5164.
[64] J.C. Phillips and J.A. Van Vechten, Phys. Rev. Lett. 30 (1973) 220.
[65] D.J. Chadi, Phys. Rev. Lett. 43 (1979) 43.
[66] J.C. Knights, Jap. J. Appl. Phys. 18 Suppl. 18-1 (1978) 101; J.C. Knights, G. Lucovsky and R.J. Nemanich, J. Non-Crystalline Solids 32 (1979) 393; J.C. Knights, J. Non-Crystalline Solids 35 (1980) 159.
[67] H.J. Stein and P.S. Peercy, Appl. Phys. Lett 34 (1979) 604; H.J. Stein, Phys. Rev. Lett. 43 (1979) 1030.
[68] H.L. Frisch, V.A. Vyssotsky, S.B. Gordon and J.M. Hammersley, Phys. Rev. 123 (1961) 1566; T.J. Coutts, Thin Solid Films 38 (1976) 313; P.L. Leath, Phys. Rev. B14 (1976) 5046.
[69] J.J. Hauser, private communication.
[70] D.E. Aspnes and A.A. Studna, to be published.
[71] D. Kaplan, N. Sol and G. Velaco, Appl. Phys. Lett. 33 (1978) 440.
[72] J.C. Bean and J.M. Poate, Appl. Phys. Lett. 36 (1980) 59; G. Foti, J.C. Bean, J.M. Poate and C.W. Magee, to be published.
[73] P.A. Thomas, M.H. Brodsky, D. Kaplan and D. Lepine, Phys. Rev. 18B (1978) 3059.
[74] G.I. Desterfanis and J.P. Gaillard, Appl. Phys. Lett. 36 (1980) 40.